NASA Technical Paper 1135

A Flight Evaluation of a Trailing Anemometer for Low-Speed Calibrations of Airspeed Systems on Research Aircraft

Bruce D. Fisher, Bruce J. Holmes, and H. Paul Stough III

FEBRUARY 1978

NASA

NASA Technical Paper 1135

A Flight Evaluation of a Trailing Anemometer for Low-Speed Calibrations of Airspeed Systems on Research Aircraft

Bruce D. Fisher, Bruce J. Holmes,
and H. Paul Stough III
Langley Research Center
Hampton, Virginia

National Aeronautics
and Space Administration
**Scientific and Technical
Information Office**
1978

SUMMARY

Research airspeed systems on three low-speed general aviation airplanes were calibrated by the trailing anemometer method. Each airplane was fitted with an NASA pitot-static pressure tube mounted on either a nose or wing boom. Flight tests were made with one airplane to study the feasibility of gathering data during a constant-rate deceleration instead of during a series of stabilized test conditions. For this aircraft, results of the calibrations with the trailing anemometer were compared with those from a version of the tower flyby method.

The research airspeed systems contained static-pressure position errors which were too large for high accuracy flight research applications. The trailing anemometer and tower flyby calibrations were in agreement for the one aircraft for which the comparison was made. The continuous deceleration technique for the trailing anemometer method offers reduced test time with no appreciable loss of accuracy for airspeed systems with pitot-static lag characteristics similar to those described in this paper.

INTRODUCTION

With the increasing use of STOL and low-speed general aviation aircraft, a need has arisen for an accurate, easy-to-use, airspeed calibration method for low airspeeds. Although the production-line airspeed systems presently used for low-speed operations may be sufficiently accurate for operational use, there is a need, for research purposes, to be able to determine airspeed precisely, even when nose or wing booms are used. For example, small errors in airspeed can produce significant differences in results of parameter extraction tests.

There are many methods for calibrating aircraft pitot-static systems that are quite accurate over a large range of airspeeds. They involve the accurate measurement of such parameters as true airspeed, total and static pressure, and geometric altitude. A brief discussion of some commonly used airspeed calibration methods is given in reference 1. Unfortunately, as pointed out in reference 1, most of these methods are not reliable at airspeeds below 60 knots because the variables generally are not measured to sufficient accuracy. At these lower airspeeds, the dynamic pressure is so low that small pressure errors become relatively significant. In fact, the measurement errors may be as large as the position error (error in the airspeed system due to the difference between the measured and free-stream pressures) of the pitot-static system. In addition, some airspeed calibration techniques can become hazardous or impractical at very low airspeeds.

The staff of NASA Langley Research Center has recently developed a self-contained, trailing anemometer system (refs. 1 and 2) which accurately measures true airspeed to as low as 7 knots. By use of this system, the position error

is determined from a comparison of the measured dynamic pressure and pressure calculated from the true airspeed, free-stream temperature, and measured static pressure; thus, the need to compare two small quantities having significant measurement error is eliminated. Further discussion of the accuracy of the trailing anemometer is given in reference 1.

The purpose of the present investigation was to evaluate the trailing anemometer technique of airspeed calibration through flight tests on three low-speed general aviation airplanes. Each airplane was fitted with an NASA pitot-static pressure tube (ref. 3) mounted on either a wing or nose boom. For one aircraft, static and dynamic test techniques were compared, and use of the trailing anemometer was compared with a version of the tower flyby method.

SYMBOLS

Except for airspeed, which is given in knots (1 knot = 0.514 m/sec), data are presented in the International System of Units (SI) with the equivalent values given parenthetically in U.S. Customary Units. The measurements and calculations were made in U.S. Customary Units. (Factors relating the two systems of units in this paper may be found in ref. 4.)

A	aspect ratio, b^2/S
B	constant used in tower flyby equations (see eq. (A9))
b	wing span, m (ft)
C_L	airplane lift coefficient, L/qS
g	local acceleration of gravity, $m\text{-}sec^{-2}$ ($ft\text{-}sec^{-2}$)
K	airspeed conversion constant, 0.514 $m\text{-}sec^{-1}\text{-}knot^{-1}$ (1.688 $ft\text{-}sec^{-1}\text{-}knot^{-1}$)
L	lift, N (lb)
M	free-stream Mach number
p	free-stream static pressure, Pa ($lb\text{-}ft^{-2}$)
p_1	static pressure from barograph on meteorological tower, Pa ($lb\text{-}ft^{-2}$)
q	dynamic pressure, $\rho V^2/2$, Pa ($lb\text{-}ft^{-2}$)
q_c	impact pressure, Pa ($lb\text{-}ft^{-2}$)
R	gas constant, 8314.34 $J\text{-}kmole^{-1}\text{-}K^{-1}$ (1716.5 $ft\text{-}lb\text{-}slug^{-1}\text{-}{}^{o}R^{-1}$)
S	wing planform area, m^2 (ft^2)
T	absolute total temperature, K (^{o}R)

T_1 absolute free-air temperature from recording thermometer on meteorological tower, K (^{o}R)

u horizontal component of induced velocity, m-sec^{-1} (knots)

V true airspeed, knots

V_c calibrated airspeed, knots

V_i indicated airspeed, knots

x horizontal distance behind aircraft, m (ft)

Z_a geometric altitude of aircraft, m (ft)

Z_1 geometric altitude of barograph used for tower flyby calibration method, m (ft)

z vertical distance below aircraft, m (ft)

α angle of attack with respect to airplane longitudinal axis, deg

Δh altitude error, m (ft)

Δp static-pressure position error, $p' - p$, Pa (lb-ft^{-2})

ΔV_c airspeed position error, $V_c - V_i$, knots

ΔZ difference between geometric altitude of aircraft and geometric altitude of barograph on meteorological tower, $Z_a - Z_1$, m (ft)

δ when used as prefix, represents random data system errors for both measured and calculated quantities

δ_f flap deflection, positive for trailing edge down, deg

ρ air density, kg-m^{-3} (slugs-ft^{-3})

Subscript:

o standard sea-level conditions

A prime denotes a probe-measured quantity.

AIRPLANES AND INSTRUMENTATION

Airplanes

The trailing anemometer system was installed on the three airplanes shown in figure 1. Airplane A (fig. 1(a)) was a high-wing, fixed-gear, twin-engine, STOL-type transport with full-span, double-slotted Fowler flaps. Airplane B

(fig. 1(b)) was a low-wing, single-engine airplane with retractable gear and partial-span, single-slotted Fowler flaps. Airplane C (fig. 1(c)) was a low-wing, retractable-gear, light twin-engine aircraft. The wing incorporated a GA(W)-1 section with full-span, single-slotted Fowler flaps, and spoilers for roll control.

A shielded total-temperature probe and the deployment mechanism of the trailing anemometer system were installed on each aircraft. On airplane A, they were attached to the bottom of the fuselage aft of the main gear. Because of the low ground clearance of airplanes B and C, the system was installed on a bracket on the side of the fuselage of each of these aircraft. The three installations are shown in figure 2. For airplanes A and B the research instrument systems utilized boom-mounted sensors: a nose-boom sensor on airplane A and a wing-boom sensor on airplane B. Airplane C utilized a single nose-boom sensor for both the cockpit and the research instrument systems.

Instrumentation

Trailing anemometer system.- True airspeed was measured by an anemometer which was trailed outside the aircraft pressure influence field. The anemometer has negligible shaft friction so that the anemometer propeller rotation speed is proportional to true airspeed without regard to air density. (See ref. 2.)

The trailing anemometer is shown in figure 3; the complete system is shown in figure 4. The basic system components are the trailing anemometer, deployment mechanism, and an operator's control box.

The anemometer (fig. 3) is mounted in a small, low-drag brass body with tail fins for self-alinement with the airstream. The anemometer is shown in the retracted position below the deployment mechanism in figures 2 and 4. The rotational speed of a small, six-bladed, low-inertia propeller is sensed with a miniature self-generating tachometer inside the anemometer body. At airspeeds above 7 knots, this rotational speed is proportional to true airspeed. Below 7 knots, the friction and magnetic forces are large enough to insure that the propeller will not reliably rotate.

The deployment mechanism is enclosed in a streamlined fiber-glass case, and is designed to be attached to the outside of an aircraft, as shown in figure 2. The deployment mechanism should be mounted on the aircraft in a region of low local turbulence to avoid exciting trailing cable oscillations at short cable lengths during retraction. Calculations predict that the cable-anemometer combination will also develop cable whipping instabilities above 165 knots true airspeed. A complete discussion of the anemometer system, installation, and operations is given in references 1 and 2.

Aircraft instrumentation systems - trailing anemometer method.- For the trailing anemometer method, static pressure, impact pressure, total temperature, true airspeed, and angle of attack were measured and recorded with time correlation onboard each of the three airplanes by magnetic tape data systems. The data system for airplane A recorded all the variables at 80 samples per

second by the pulse-code-modulated method. On airplane B, true airspeed, total temperature and static pressure were sampled 10 times per second by a pulse-amplitude-modulated commutator; impact pressure and angle of attack were measured continuously. All data on airplane B were recorded on a frequency-modulated system. On airplane C, the data were recorded on a frequency-modulated, 14-track magnetic tape data acquisition system with one track commutated for 28 additional channels. Impact pressure, static pressure, and total temperature were sampled 10 times per second by a pulse-amplitude-modulated commutator; angle of attack and true airspeed were measured continuously. For all three aircraft, the data were processed at 10 samples per second.

Each measurement contained random data system errors from the sensors, airborne recorders, and data reduction system. The variables, with their ranges and random data system errors, are given for each airplane data system in table I. The values for the random data system errors were best estimates of the data system capabilities. Effects of nonlinearity were eliminated in the data reduction process. Drift was minimized by preflight calibrations. The effects of the random data system errors are discussed in the data reduction section of this paper and the method of calculating these effects is described in the appendix.

Static pressure and impact pressure were sensed by transducers connected to an NASA pitot-static and flow-direction pressure tube shown in figure 5. The pressure tube was approximately 1.5 fuselage diameters ahead of the nose of airplane A, and 1.0 fuselage diameter ahead of airplane C. On airplane B, the pressure tube was mounted on a wing-tip boom at 0.99 wing-tip chord ahead of the leading edge. (See fig. 1.) The pressure tube was designed to minimize the effects of flow angularity on total and static-pressure measurements. The performance (refs. 3 and 5) and location (ref. 6) data for this pressure tube confirmed that there was negligible error in the measured total pressure. Therefore, all the position error in research pitot-static systems was assumed to be static-pressure position error due to the presence of the aircraft.

Air temperature was measured by a shielded total-temperature probe. The temperature sensed by the probe was essentially the same as the free-air temperature, with insignificant loss of accuracy for the airspeeds tested ($M \leqq 0.2$). The true airspeed was sensed by the trailing anemometer. The anemometer was calibrated to an accuracy of ± 0.5 knot in a wind tunnel, but the flight accuracy including the random data system errors was estimated to be about ± 1 knot for airplanes A and C and ± 3 knots for airplane B. (See table I.) Angle of attack, sensed by a vane mounted aft of the static orifices on the instrumentation booms, was corrected for local flow errors.

The effect of lag in the pitot-static system of airplane C was measured to insure that the time-dependent behavior of the system would not distort the wave form and would allow correlation of all parameters during the dynamic maneuvers (decelerations) performed with this airplane. The static-system lag-time constant was 0.183 sec; the pitot lag was much smaller. The procedure used to determine the lag characteristics are given in reference 7. The lag found resulted in less than 1.0-percent static-pressure error ($(\Delta p/q_c') < 0.01$) for dynamic maneuvers where the rate of change of airspeed was less than about

1 knot/sec at constant altitude, or a rate of change of altitude less than 2 m/sec (400 ft/min) at constant airspeed.

Airborne and ground-based instrumentation - tower flyby method.- For the tower flyby airspeed calibration of airplane C, both airborne and ground-based measurements were used. Static pressure, impact pressure, total temperature, and angle of attack were recorded with time correlation onboard the airplane in the same manner as in the trailing anemometer method, except that impact pressure and static pressure were recorded continuously rather than by the commutator. The data were processed at 10 samples per second.

A schematic of the test equipment is given in figure 6. A three-dimensional time history of aircraft position, from which airplane altitude was taken, was produced by a ground-based radar. Static pressure and free-air temperature were measured by barographs and recording thermometers at three elevations on a 76.2-m (250-ft) meteorological tower used for the flybys. On each run, the values of pressure and temperature at the sensor elevation on the tower nearest the radar-measured altitude of the airplane were used as the datum to compute the true static pressure at the airplane's altitude. The airborne and ground-based variables are listed in table II with their corresponding ranges and random data system errors. The angular precision of the ground-based radar was ± 0.5 mil root mean square, which gave a radar altitude precision of ± 0.2 m (0.5 ft) for the nominal radar range to the airplane (3287.6 m) during the flyby test runs. The effects of the random data system errors are discussed in the data reduction section of this paper and the methods of calculating these effects are described in the appendix.

EXPERIMENTAL METHODS AND TESTS

Trailing Anemometer Method

Measurements.- In the trailing anemometer method, all the variables are measured onboard the aircraft. The static-pressure position errors are computed from the values of static pressure, impact pressure, and total temperature measured by aircraft-mounted sensors, and true airspeed measured by the trailing anemometer. An advantage of the method is that the equations use the measured values of static and impact pressure to compute the static-pressure position error. The method is limited to speeds at which the effect of compressibility is negligible.

Trailing cable length.- Any trailing calibration sensor, whether a pressure probe or an anemometer, must be trailed outside the aircraft pressure influence field to sense the characteristics of the undisturbed free stream. The normalized induced velocity u/V that would be measured by a trailing sensor is given in figure 7 as a function of the sensor position below and behind the aircraft for two airplane conditions (low speed with flaps down, and high speed with flaps up). The anemometer trail position is also shown for these two conditions. The curves of induced velocity ratio were determined by the method of reference 8, and the anemometer positions were based on the method of reference 1, a deployed cable length of 30.5 m (100 ft) being assumed.

Considerably more cable needs to be deployed to have the anemometer in relatively undisturbed air for high-lift (low-speed) conditions than for low-lift (high-speed) conditions. For example, with the anemometer deployed along the u/V curves which pass through $x/b = z/b = 0.4$, the induced velocity ratio would be -0.25×10^2 for the high-speed, low-lift condition, and -2.0×10^2 for the low-speed, high-lift condition. The data of reference 8 indicate that trailing the anemometer at a radius of 1.5 wing spans from the aircraft will result in negligible induced velocity error. For the airspeeds and airplanes used in these tests, the cable lengths were chosen by using this criterion to insure that the induced flow errors were insignificant.

Tests.- Airspeed calibration data were taken for all three airplanes at constant speed and altitude conditions (the steady-run technique). At the desired test altitude, the anemometer was deployed below and behind the airplane. At each test condition, data were recorded in straight, level, unaccelerated flight with the power required for level flight at that speed. The data used for each condition were the averaged values of the recorded variables from a steady-state period of each test run.

A total of 15 test runs were made with airplane A, consisting of 5 flaps-up runs between 70 and 88 knots and 10 flaps-down runs between 44 and 82.5 knots. The lowest speed point in each configuration for airplane A was near the stall. Airplane B was calibrated over a speed range of 74 to 109 knots with flaps up, and a range of 65 to 109 knots with flaps down. The lowest speed for each configuration for airplane B was just above the stall buffet. The flap-down calibrations were made at two cable lengths. Seventeen runs were made with airplane B. Only three steady-calibration runs were made with airplane C, with the gear and flaps up and the speed ranging from 75 to 110 knots. The steady-run test conditions for the three airplanes are summarized in table III.

Continuous position-error calibration data were gathered on airplane C by two techniques: decelerations with throttles fixed, and decelerations with throttles gradually retarded. Fixed-throttle decelerations produced data which were used to evaluate the effects of power on static-pressure position error. Decelerations with throttles gradually retarded were used to generate quasi-steady-state data for comparison with steady-state data points. Decelerations were continued through the stall.

During the decelerations, a simple form of quality control of the data was accomplished by timing the duration of the maneuver to determine that the average flight-path deceleration was less than 1 knot/sec, and that the average rate of descent was less than 2 m/sec (400 ft/min). Decelerations and rates of descent less than these values insured that the pitot-static system pneumatic lag was inconsequential. It was also necessary that the throttle be smoothly retarded. Rough retardation of the throttles produces fore-and-aft swinging of the anemometer and thus oscillations in the true airspeed records result. Time histories of static-pressure position error with angle of attack were computed from the recorded time-history data. The conditions for the seven deceleration runs made with airplane C are given in table III.

Tower Flyby Method

Airspeed calibrations by the tower flyby method are made by comparing flight measured static pressure with the correct ambient pressure from tower measurements. The key element of the tower flyby method is the determination of the geometric height of an aircraft above a known reference at a particular time. The ambient static pressure at the aircraft altitude is determined from the pressure measured at the reference datum and adjusted to the airplane height by a standard lapse rate correction. This computed "correct" value is then compared with the static pressure measured on the aircraft, the difference being the static-pressure error. The procedure for the tower flyby consisted of trying to fly the airplane at the same geometric altitude as a fixed-barometric pressure recording device. The precise altitude was determined from radar records from a ground-based radar system.

Ideally, each run was made in steady, level flight. In reality, it was difficult to hold both altitude and airspeed. Of the two, airspeed was allowed to vary because the determination of altitude was critical to the overall accuracy of this method. The importance of accurate altitude measurement for the tower flyby method is discussed in the section "Data Reduction."

Calibration of static-pressure error by the tower flyby technique was restricted by safety considerations to speeds above 85 knots (25 knots above stall speed, flaps up). A safe margin above stall speed was required because of the proximity of the airplane to the ground during the passes by the meteorological tower. At airspeeds below 85 knots (flaps up), it became difficult to maintain the required level constant-altitude flight past the tower.

All tower flyby tests were conducted with flaps and gear up. The test conditions for the three tower flyby runs for airplane C are summarized in table III(c).

DATA REDUCTION

General Assumptions

Two basic assumptions were made for the trailing anemometer and tower flyby methods. First, for the low speeds used in these tests, the airflow was assumed to be incompressible. Second, it was assumed that all position error in the research airspeed systems was static-pressure position error Δp due to the pressure influence fields of the airplanes. The static-pressure position error is the difference between the measured and the actual static pressure $\Delta p = p' - p$. Actually, Δp also included small flow angularity error in static pressure due to the characteristics of the NASA airspeed tube; but, since the entire airspeed system was being calibrated, this error was simply included as part of the static-pressure position error.

A detailed presentation of the effects on calibration accuracy of random data system errors in the variables is given later in this paper and in the appendix. No corrections were made to the data for center-of-gravity position because the center-of-gravity variations for the three airplanes were so small.

Trailing Anemometer Method

Equations given in reference 1 show how pressure, temperature, density, and velocity relations have been combined to give the following expression for static-pressure position error:

$$\Delta p = \frac{(p'V^2K^2/2RT') - q_c'}{1 + (V^2K^2/2RT')}$$

This expression does not require measurement of free-stream static pressure. Instead, the free-stream state is established through measurement of true airspeed by the trailing anemometer. The measured impact pressure q_c' and the measured static pressure p' were sensed by the research airspeed systems, and the measured total temperature T' sensed by a probe on the aircraft was essentially equivalent to free-stream temperature, as discussed in reference 1.

The static-pressure position error was then used to determine the following:

(a) Calibrated airspeed

$$V_c = V\sqrt{\frac{(p' - \Delta p)T_o}{p_o T'}} \tag{1}$$

(b) Impact pressure

$$q_c = q_c' + \Delta p$$

(c) Static pressure

$$p = p' - \Delta p$$

Indicated airspeed was computed by the relation:

$$V_i = \frac{1}{K}\sqrt{\frac{2q_c'}{\rho_o}} \tag{2}$$

As defined in reference 9, calibrated airspeed is indicated airspeed corrected for instrumentation and position errors. Since, for the research airspeed systems, indicated airspeed was computed from recorded pressure q_c', there were no instrument calibration errors. Therefore, the difference between calibrated and indicated airspeed for these systems is the static-pressure position error in terms of airspeed:

$$\Delta V_c = V_c - V_i \tag{3}$$

Each steady-state run produced a single calibration point representing that particular test airspeed and configuration. On the other hand, for each deceleration maneuver (airplane C), the time-correlated values of each measured variable produced a continually varying set of data.

In order to handle the data sample rate (10 samples per second) from the deceleration calibration maneuvers, the data reduction method was programed for a high-speed digital computer to average and smooth the data over selected time intervals of the test run. The resulting data could be either manually faired or numerically curve fitted. Data presented in this paper were manually faired.

Tower Flyby Method

As was the case for the trailing anemometer method, static pressure containing position error p' was measured onboard the airplane by the research airspeed system. However, for the tower flyby method, the reference static pressure p was determined from a barograph recording of ambient pressure corrected for airplane altitude relative to the barograph.

In the tower flyby test runs, the difference between the airplane altitude and the closest barographic device in the tower averaged about 4 m (13 ft). To obtain the reference static pressure p at the airplane geometric height, a standard lapse-rate correction was applied to the barograph-recorded static pressure p_1 by a form of the hydrostatic equation:

$$p = p_1 \exp \frac{-\Delta Z}{RT'}$$

Calibrated airspeed V_c was computed by the relation

$$V_c = \frac{1}{K}\sqrt{\frac{2q_c}{\rho_o}} = \sqrt{\frac{2(q_c' + \Delta p)}{\rho_o}}$$

The static-pressure position error was the difference between p and the static pressure measured with the airplane nose boom p' at the time of tower passage; that is,

$$\Delta p = p' - p$$

Indicated airspeed V_i and airspeed position error ΔV_c were determined by the relations utilizing temperature T' and measured impact pressure q_c' measured onboard the airplane. (See eqs. (1) to (3).)

Effect of Random Data System Errors on Calibration Accuracy

The derivation of the equations for computing airspeed errors equivalent to the random data system errors for the trailing anemometer and tower flyby methods is given in the appendix of this paper. A comparison of the effects

of random data system errors for the trailing anemometer and tower flyby methods is presented in table IV. The ranges of the airborne measurements for both methods for this example are taken from the instrumentation system of airplane A (table I(a)), as they are considered to be representative of a high accuracy installation. The ranges for the ground-based measurements are taken from table II. With the exception of altitude Z_a, it was assumed that the random data system errors were 1 percent of the full-scale range of each instrument. The random error for Z_a was based on the radar angular resolution and nominal distance. The random data system errors in table IV were converted to errors in airspeed at $V = 100$ knots by using the assumptions and method outlined in the appendix. To isolate the effects of the random data system errors, it was also assumed that the static-pressure position error was zero. For this example, the combined root-mean-square (rms) data system error for the trailing anemometer method is about one-fifth of the corresponding rms error for the tower flyby method. This difference in overall accuracy is even more pronounced at lower airspeeds.

The measurement of static pressure is critical to the accuracy of the tower flyby method. In the tower flyby example in table IV, a random error in static pressure $\delta p'$ of ± 170.5 Pa (± 3.56 lb/ft^2) was equivalent to an airspeed error of ± 5.23 knots. The same $\delta p'$ in the trailing anemometer example was equivalent to an airspeed error of only ± 0.08 knot.

The pressure sensitivity in the tower flyby method is also reflected in the measurement of local barometric pressure p_1 and, to a smaller extent, aircraft geometric altitude Z_a. Based on a standard lapse rate, altitude error is related to static-pressure error in figure 8, which presents the normalized position error $\Delta p/q$ as a function of true airspeed V. The figure illustrates that a relatively small static-pressure variation derived from an altitude error rapidly becomes a significant part of the measured dynamic (or impact) pressure at low speeds. An error in static pressure p or p_1 in the tower flyby method will affect the airspeed calibration at lower airspeeds in a similar fashion to the altitude errors shown in figure 8. Sensitivity to errors in static-pressure measurement in the trailing anemometer method is minimized by utilizing calculated terms based on true airspeed and total temperature. This is one of the prime advantages of the trailing anemometer method.

The sensor ranges and random data system errors for the variables used in the trailing anemometer method are summarized in table I for the three airplanes. The sensor ranges and random data system errors for the airborne and ground-based instrumentation for the tower flyby calibration of airplane C are summarized in table II. For each airplane, airspeed errors were computed by the method in the appendix for two sample airspeeds representing the high and low ends of the airspeed calibration ranges. As was the case in table IV, the static-pressure position error was assumed to be zero, and the airspeed errors were computed for the same atmospheric conditions as assumed for table IV. The rms accuracies for the trailing anemometer method (table I) varied from ± 3.0 knots at $V = 50$ knots with the instrumentation system of airplane C to ± 0.53 knot at $V = 100$ knots for airplane A. These accuracies are generally adequate for precision low-speed calibrations.

The rms error for the tower flyby calibration of airplane C (table II) varied from ±1.3 knots at V = 170 knots to ±2.6 knots at V = 90 knots. A static-pressure transducer with a $\delta p' = \pm 170$ Pa was used in the tower flyby calibration of airplane C. In comparison, the sea-level rms error for the trailing anemometer method with airplane C was still only ±1.6 knots at V = 50 knots, even though a relatively insensitive static-pressure transducer ($\delta p' = \pm 2070$ Pa) was used in the anemomenter tests (table I(c)).

By reference to table IV, at airspeeds of 100 knots, a high-quality instrumentation system giving random data system errors of 1-percent full-scale range results in a combined rms data system error of ±2.44 knots for airspeed calibrations by the tower flyby method. The same instrumentation system can give a combined rms data system error of ±0.53 knot for airspeed calibrations by the trailing anemometer method, when true airspeed is measured within ±1 knot.

RESULTS AND DISCUSSION

Airplane A

Figure 9 illustrates the scatter in the data points. Since the shape of the curve of position error plotted against angle of attack is not well known, the raw data were plotted, as shown in figure 10, as a variation of $1/q_c$ and $1/q_c'$ with α. These curves can be faired easily, having the recognizable shape of the variation of C_L against α. Values from these faired curves were then used to determine the faired value of the static-pressure position error curve (fig. 9) based on the relation

$$\frac{\Delta p}{q_c'} = \frac{(1/q_c') - (1/q_c)}{1/q_c}$$

The trends of the static-pressure position errors shown in figure 9 agree generally with the data given in references 5 and 6 for a nose-boom probe with the pressure orifices located 1.5 fuselage diameters ahead of the aircraft nose. With flaps up and $\alpha = 8^\circ$, the curve of figure 9 shows $\frac{\Delta p}{q_c'} = 0.0515$, which is equivalent to a $\frac{\Delta p}{q_c} = 0.0485$. For the same angle-of-attack and probe location, the data of reference 5 gave a $\frac{\Delta p}{q_c} = 0.045$ for a probe ahead of a hemispherical nose and a $\frac{\Delta p}{q_c} = 0.025$ for a probe ahead of a parabolic nose. The value based on the data from figure 9 does not fall between these values, even though the shape of the nose of airplane A falls between the two shapes of reference 5. The discrepancy exists because the data in reference 5 do not include the effects of wing flow, engine power, or flap deflection. In fact, no data exist which allow accurate prediction of $\Delta p/q_c'$ for a given airplane configuration with varying angle of attack, Mach number, and flap deflection.

In figure 9, it can be seen that flap deflection produces a pronounced negative shift in static-pressure position error, which should be expected since the lift coefficient is significantly greater at a given angle of attack when the flaps are deflected. It is apparent that the full-span double-slotted Fowler flaps influence the flow field even at a probe location 1.5 body diameters ahead of the nose of the airplane.

The static-pressure position error in terms of calibrated airspeed is shown in figure 11. The maximum position errors in terms of calibrated airspeed are about ± 2.5 knots; in terms of pressure (fig. 9), the maximum errors range from 7 to -9 percent of the measured impact pressure. It was shown in reference 1 that between indicated angles of attack of $\pm 4^{\circ}$, which is the normal, full-flap approach operating range of airplane A, the static-pressure position errors of the research airspeed system were about one-half of those of the standard airplane airspeed installation in terms of airspeed. However, the research airspeed-system position errors and the standard airplane-airspeed-system position errors still represent consistent and measurable errors which can be calibrated by the trailing anemometer method.

Airplane B

The variation of static-pressure position error with angle of attack for airplane B (flaps up and flaps down) is shown in figure 12. The position error curves were generated by using the technique discussed for airplane A. The variations of pressure error with angle of attack are similar to those of the wing-boom data of reference 6. Position error increased with angle of attack to a maximum of 12.5 percent of q_c'. Based on the work of references 6 and 10, smaller errors were anticipated.

The data in figure 12 show no appreciable difference in $\Delta p/q_c'$ at a given angle of attack due to flap deflection. This may be attributed to the less effective flap system on airplane B (partial-span, single-slotted, Fowler flaps).

As discussed previously, a sensor should be deployed at least 1.5 wing spans from the airplane to measure free-stream conditions. Figure 13, however, shows that no significant change in airspeed calibration was noted by increasing the deployed cable length of the trailing anemometer from 1.4 to 2.8 wing spans of airplane B.

The position-error data for airplane B in terms of calibrated airspeed for both flap configurations and cable lengths are combined and represented by a single faired curve in figure 14. The scatter in the data relative to the curve is within the combined rms data system errors given in table I(b). The calibrated airspeed error using the faired curve for airplane B ranged between -3.8 and -1.2 knots for indicated airspeeds between 65 and 109 knots, respectively, for either flaps up or down.

Airplane C

Trailing anemometer calibrations.- As previously discussed, a deceleration technique was used for airplane C. It was found in these tests that the quality of the data from the decelerations was heavily dependent on pitot-static system lag, and on the smoothness of the deceleration. As long as the rate of change of airspeed was less than 1 knot/sec, and the rate of change of altitude was less than 2 m/sec (400 ft/min), pitot-static system lag was negligible. If the deceleration did not occur smoothly, the anemometer tended to develop a swinging motion which produced oscillating true airspeed data.

Figure 15 shows the variation of static-pressure position error with indicated airspeed for two sample decelerations. The pressure errors were computed from the raw true airspeed data. These pressure errors were effectively filtered by fitting the data with a polynomial routine to illustrate anemometer swing. In the deceleration shown in figure 15(a), the throttles were not retarded smoothly, and the trailing anemometer developed a swinging oscillation. The swing is evident by the loops and discontinuities in the data. The data in figure 15(b) were taken from a smooth deceleration, and the variation of static-pressure error with V_i is smoother.

When using the steady run variant of the trailing anemometer method, it is recommended that increments between data points be reduced as angle of attack is increased, particularly near the stall. Close spacing of data near the stall will facilitate curve fitting. The use of dynamic maneuvers is advantageous in that they generate uninterrupted data files which can be sampled at any interval desired.

Data in figure 15(b) were manually faired and are given in figure 16, which shows the variation of static-pressure position error with angle of attack for the nose-boom probe system of airplane C. The figure includes data from both steady runs and decelerating maneuvers. For all flap conditions, the maximum static-pressure error ranged from 2 to about -6 percent of q_c' over the angle-of-attack range of the calibration. This range of position error is similar to those for the research airspeed systems on airplanes A and B. It was estimated that the flight time required to complete an airspeed calibration with the trailing anemometer could be reduced by a factor of 10 if the decelerating maneuvers were used instead of the series of discrete runs.

The influence of flap deflection on static-pressure position error for a given angle of attack is also shown in figure 16. The increase in lift coefficient due to flap deflection produces a negative shift in position error up to $\delta_f = 30^\circ$, and then no further change.

The effect of engine power on static-pressure position error can be seen in figure 17, which shows the variation of $\Delta p/q_c'$ with α for $\delta_f = 0^\circ$ and 30°. The curves appear to show opposite effects of power on position error with flap deflection; that is, with $\delta_f = 0^\circ$, a decrease in power shows increased rate of change of $\Delta p/q_c'$ with α, whereas with $\delta_f = 30^\circ$, decreased power tends to decrease the rate of change of $\Delta p/q_c'$ with α. The reasons for the difference in effect of engine power on static-pressure position error are not known.

The differences between the three steady runs and the decelerating calibration for $\delta_f = 0^o$ fall within the combined rms data system errors given in table I(c). The scatter in raw (unsmoothed) data gathered in steady runs is illustrated by the bars in figure 18(a). The figure shows that the continuous data gathered during the decelerating maneuvers fall well within the limits of the raw data scatter. It is felt that there is essentially no loss of accuracy with the decelerating maneuver variation in comparison to the steady run variation of the trailing anemometer method.

Tower flyby calibration.- The results of the three tower flyby runs with airplane C are plotted in figure 18 with the corresponding results from the trailing anemometer method. The variation of $\Delta p/q_c'$ with α is shown in figure 18(a), and the equivalent variation of ΔV_c with α is plotted in figure 18(b). The tower flyby calibration shows essentially zero static-pressure position error over the angle-of-attack range used; however, the angle-of-attack range proved to be too narrow to show the variation of position error with angle of attack.

The trailing anemometer and tower flyby calibrations were in agreement within the accuracies of the methods at the tower flyby speeds. The speeds for the tower flyby runs were high enough (see table III) to insure that the combined rms data system errors for this method (table II) are close to those for the trailing anemometer method (table I(c)) for airplane C. Of the numerous tower flyby runs performed, only three produced usable data, which appear in figure 18 and in table III. The remaining runs were discarded because of the uncertainty in altitude at tower passage. At lower speeds, the tower flyby results would not be reliable because of the rapid deterioration of calibration accuracy at low speeds for those methods which require an accurate measurement of geometric altitude or static pressure. Not only was the trailing anemometer method more accurate, it was also found to be appreciably easier to use than the tower flyby method, because the trailing anemometer system was self-contained.

Comparison of Results

Even though the aircraft tested employed research airspeed systems mounted on rather long instrumentation booms (1.5 and 1.0 fuselage diameters for nose booms and 0.99 chord length for the wing boom) to minimize position errors in pressure measurements, the static-pressure position errors for the three research airspeed systems fell between ± 10 percent of measured impact pressure (figs. 9, 12, 13, 16, and 17), with corresponding errors in calibrated airspeed that fell between 2.5 and -5 knots (figs. 11, 14, and 18). The largest low-speed (large α and C_L) position errors were found in the research airspeed systems on airplanes A and B. One of the research airspeed systems with the NASA pitot-static tube mounted on a nose boom (airplane A) contained position errors equivalent to -2.5 knots at speeds as low as $V_i = 46.1$ knots ($\alpha = 7.3^o$, flaps down). The research airspeed system on airplane B, in which the tube was mounted on a wing boom, contained position errors equivalent to about -4 knots at $V_i = 65.2$ knots ($\alpha = 9.5^o$, flaps down). These position errors are small enough to insure that the uncalibrated research airspeed systems are adequate as installed for many operational and flight-test applications. However, the

static-pressure position errors found in these three systems are too large for some flight research applications, such as parameter identification. The systems must be calibrated before they can be used for such purposes. Reference 1 has shown that the trailing anemometer is one of the few techniques capable of detecting small pressure errors such as those in the three systems tested. The data scatter caused by the inherent inaccuracies of other calibration methods would mask these small position errors. In particular, the tower flyby method is not suitable for precision airspeed calibrations at low airspeeds ($M < 0.2$).

The results of these tests suggest a reevaluation of the use of long instrumentation booms, since the installation is difficult because they cannot be easily stiffened to avoid a low natural bending response. The accuracy of a calibrated pressure source should be the same whether mounted on a long or short boom when the trailing anemometer method is used. (See ref. 1 for comparison of nose boom and production airspeed systems for airplane A.) Therefore, the use of long pitot-static booms for the purpose of minimizi position errors may not be justified.

SUMMARY OF RESULTS

Research airspeed systems on three low-speed general aviation airplanes were calibrated by using the trailing anemometer method. Each airplane was fitted with an NASA pitot-static pressure tube mounted on either a nose or a wing boom. For one airplane, comparisons were made between static and continuous deceleration techniques with the trailing anemometer, and between tower flyby and trailing anemometer techniques. The results of the tests indicated that:

1. Appreciable position errors can exist in boom-mounted research-airspeed systems and can be determined by the trailing anemometer calibration method. A research airspeed system utilizing an NASA pitot-static head mounted 1.5 fuselage diameters ahead of an aircraft nose was shown to contain position errors equivalent to -2.5 knots at speeds as low as 46.1 knots. A research airspeed system on another airplane with the head mounted 0.99 chord ahead of the wing tip contained position errors equivalent to about -4 knots at an indicated velocity of 65.2 knots.

2. At low airspeeds (Mach number < 0.2), the tower flyby method is not suitable for precision airspeed calibrations.

3. The trailing anemometer and tower flyby calibrations were in agreement within the accuracies of the methods at the tower flyby speeds. However, the trailing anemometer method was more accurate and appreciably easier to use than the tower flyby method.

4. The results of these tests suggest a reevaluation of the use of long instrumentation booms. The accuracy of a calibrated pressure source should be the same, whether mounted on a long or short boom when the trailing anemometer calibration method is used. Therefore, the use of long pitot-static booms for the purpose of minimizing position errors may not be justified.

5. Airspeed boom installations can be affected by flap deflection. For two nose-probe systems fitted to aircraft with full-span Fowler flaps, a negative shift in position error at a given angle of attack with increasing flap deflection was shown. No effect of flap deflection was seen one chord ahead of the wing tip of an aircraft with partial-span Fowler flaps.

6. No significant change in airspeed calibration was noted by increasing the deployed cable length of the trailing anemometer from 1.4 to 2.8 wing spans on the aircraft with partial-span Fowler flaps.

7. The continuous deceleration variant of the trailing anemometer method offers reduced test time with no appreciable loss of accuracy for airspeed systems which have small pitot-static system lag.

Langley Research Center
National Aeronautics and Space Administration
Hampton, VA 23665
December 20, 1977

APPENDIX

DETERMINATION OF AIRSPEED ERRORS CAUSED BY RANDOM DATA SYSTEM ERRORS

As discussed in the paper, the measured quantities used for the two airspeed calibration techniques contain random data system errors. These errors are related to the physical characteristics of the sensors and the data recording and processing systems.

The expressions relating these random errors to airspeed measurement error are developed in this appendix for both the trailing anemometer and tower flyby methods of airspeed calibration.

Trailing Anemometer Method

The four measured quantities used in the trailing anemometer technique are p', q_c', T', and V. As discussed in reference 1, free-stream temperature and measured total temperature T' may be assumed to be equal at the low airspeeds used in these tests. The differences between free-stream and total temperature, and the instrument error in the total-temperature probe are negligible. Therefore, the effects of random data system error on the measured temperature are not analyzed further, since these values are within the errors involved in assuming that measured total temperature T' is equal to free-air temperature.

Using the symbol δ to represent random errors (measured and calculated), the actual values used in the determination of static-pressure position error Δp are

Measured static pressure = $p' + \delta p'$

Measured impact pressure = $q_c' + \delta q_c'$

Measured true airspeed = $V + \delta V$

Measured total temperature = $T' + \delta T' \approx T'$ or Free-air temperature $\approx T'$

The static-pressure position error is

$$\Delta p = \frac{(p'V^2K^2/2RT') - q_c'}{1 + (V^2K^2/2RT')} = \frac{p'V^2K^2 - 2RT'q_c'}{2RT' + V^2K^2} \tag{A1}$$

The measured quantities used to determine position error Δp from equation (A1) contain random data system errors $\delta p'$, $\delta q_c'$, and δV. Correspondingly, the static-pressure position error determined will also have an error $\delta(\Delta p)$ so that

$$p + \delta(\Delta p) = \frac{(p' + \delta p')(V + \delta V)^2K^2 - 2RT'(q_c' + \delta q_c')}{2RT' + (V + \delta V)^2K^2}$$

Expanding this relation, combining terms, and neglecting products of small quantities gives

$$\Delta p + \delta(\Delta p) = \frac{K^2 p' V^2 - 2RT' q_c' + (2K^2 p' V \delta V) + \delta p' V^2 K^2 - \delta q_c' 2RT'}{2RT' + K^2(V^2 + 2V\delta V)}$$

The denominator of this term

$$2RT' + K^2(V^2 + 2V\delta V)$$

may be approximated as

$$2RT' + K^2 V^2$$

since the actual value of $2RT'$ is about four orders of magnitude greater than $2K^2 V \delta V$. This assumption will allow us to decouple the random error terms so that

$$\Delta p + \delta(\Delta p) = \frac{1}{2RT' + K^2 V^2}(K^2 p' V^2 - 2RT' q_c') + \frac{1}{2RT' + K^2 V^2}(2K^2 p' V \delta V + V^2 K^2 \delta p' - 2RT' \delta q_c')$$

which by equation (A1) becomes

$$\Delta p + \delta(\Delta p) = \Delta p + \frac{1}{2RT' + K^2 V^2}(2K^2 p' V \delta V + V^2 K^2 \delta p' - 2RT' \delta q_c')$$

Therefore, the effect of random data system errors of the measured variables on static-pressure position error is

$$\delta(\Delta p) = \frac{1}{2RT' + K^2 V^2}(2K^2 p' V \delta V + V^2 K^2 \delta p' - 2RT' \delta q_c') \qquad (A2)$$

Static pressure p used to determine calibrated airspeed V_c is determined from the relation

$$p = p' - \Delta p$$

and contains random errors given by the expression

$$p + \delta p = (p' + \delta p') - [\Delta p + \delta(\Delta p)]$$

which can be expressed as

$$p + \delta p = p + \delta p' - \delta(\Delta p)$$

By use of equation (A2)

$$\delta p = \delta p' - \frac{1}{2RT' + K^2V^2}(2K^2p'V\delta V + V^2K^2\delta p' - 2RT'\delta q_c') \tag{A3}$$

True airspeed from the anemometer is converted to calibrated airspeed for comparison with indicated airspeed from the NASA pitot-static pressure tube by the relation

$$V_c = V\sqrt{\frac{pT_o}{p_oT}}$$

When random errors are included, this relation becomes

$$V_c + \delta V_c = (V + \delta V)\sqrt{\frac{(p + \delta p)T_o}{p_oT}}$$

and by factoring

$$V_c + \delta V_c = (V + \delta V)\sqrt{\frac{pT_o}{p_oT}}\sqrt{1 + \frac{\delta p}{p}}$$

Expanding the second radical in this equation by a binomial series, and discarding the higher order terms, gives

$$V_c + \delta V_c = \sqrt{\frac{pT_o}{p_oT}}(V + \delta V)\left(1 + \frac{1}{2}\frac{\delta p}{p}\right)$$

or

$$V_c + \delta V_c = \sqrt{\frac{pT_o}{p_oT}}\left(V + \frac{V}{2}\frac{\delta p}{p} + \delta V + \frac{1}{2}\frac{\delta p}{p}\delta V\right)$$

or

$$V_c + \delta V_c = V_c + \sqrt{\frac{pT_o}{p_o T}}\left(\frac{V}{2}\frac{\delta p}{p} + \delta V + \frac{1}{2}\frac{\delta p}{p}\delta V\right)$$

The product of small quantities may also be dropped as a higher order term with negligible loss of accuracy, giving

$$V_c + \delta V_c = V_c + \sqrt{\frac{pT_o}{p_o T}}\left(\frac{V}{2}\frac{\delta p}{p} + \delta V\right) \tag{A4}$$

Indicated airspeed V_i was computed from the impact pressure sensed by the boom-mounted NASA pitot-static pressure tube by the equation

$$V_i = \frac{1}{K}\sqrt{\frac{2q_c'}{\rho_o}}$$

When random error in q_c' is included, the relation for V_i becomes

$$V_i + \delta V_i = \frac{1}{K}\sqrt{\frac{2(q_c' + \delta q_c')}{\rho_o}}$$

Factoring this equation yields

$$V_i + \delta V_i = \frac{1}{K}\sqrt{\frac{2q_c'}{\rho_o}}\sqrt{1 + \frac{\delta q_c'}{q_c'}}$$

which may be expressed as

$$V_i + \delta V_i = V_i\sqrt{1 + \frac{\delta q_c'}{q_c'}}$$

By using a binomial series expansion on the radical and dropping the higher order terms, the equation for $V_i + \delta V_i$ becomes

$$V_i + \delta V_i = V_i\left(1 + \frac{\delta q_c'}{2q_c'}\right) \tag{A5}$$

APPENDIX

The airspeed position error in terms of airspeed is

$$\Delta V_c = V_c - V_i$$

which actually contains random data system errors so that

$$\Delta V_c + \delta(\Delta V_c) = V_c + \delta V_c - (V_i + \delta V_i)$$

From equations (A4) and (A5),

$$\delta(\Delta V_c) = \delta V_c - \delta V_i = \sqrt{\frac{pT_o}{p_o T}}\left(\frac{V}{2}\frac{\delta p}{p} + \delta V\right) - V_i\left(\frac{\delta q_c'}{2q_c'}\right)$$

Substituting the expression for δp from equation (A3) yields

$$\delta(\Delta V_c) = \sqrt{\frac{pT_o}{p_o T}}\left\{\frac{V}{2p}\left[\delta p' - \frac{1}{2RT' + K^2V^2}(2K^2p'V\delta V + K^2V^2\delta p' - 2RT'\delta q_c')\right]\right.$$

$$\left. + \delta V\right\} - \frac{V_i}{2q_c'}\delta q_c'$$

By grouping terms, the general expression for random data system errors in terms of airspeed becomes

$$\delta(\Delta V_c) = \sqrt{\frac{pT_o}{p_o T}}\frac{V}{2P}\left(1 - \frac{K^2V^2}{2RT' + K^2V^2}\right)\delta p' + \sqrt{\frac{p}{p_o}\frac{T_o}{T}}\left[1 - \frac{1}{p}\left(\frac{K^2p'V^2}{2RT' + K^2V^2}\right)\right]\delta V$$

$$+ \sqrt{\frac{p}{p_o}\frac{T_o}{T}}\frac{VRT'}{p}\frac{1}{2RT' + K^2V^2}\delta q_c' - \frac{V_i}{2q_c'}\delta q_c' \qquad \text{(A6)}$$

The first three terms of equation (A6) will decrease with increasing altitude as the static pressure decreases.

Tables I and IV present examples of airspeed errors caused by random data system errors. Two assumptions were made in these computations. First, to isolate the effects of random data system errors, it was assumed that static-pressure position error was zero. Second, standard sea-level conditions were assumed as a conservative common condition for comparison purposes.

These assumptions permitted the following simplifications:

$$V_c = V_i = V$$

$$q_c' = q_c$$

$$p' = p = p_o$$

$$T' = T_o$$

The general expression for random error (eq. (A6)) now simplifies to

$$\delta(\Delta V_c) = \frac{V\delta p'}{2p_o}\left(1 - \frac{K^2V^2}{2RT_o + K^2V^2}\right) + \delta V\left(1 - \frac{K^2V^2}{2RT_o + K^2V^2}\right) + V\delta q_c'\left[\frac{RT_o}{p_o(2RT_o + K^2V^2)} - \frac{1}{2q_c}\right]$$

or

$$\delta(\Delta V_c) = \frac{RT_oV}{2RT_o + K^2V^2}\frac{\delta p'}{p_o} + \frac{2RT_o}{2RT_o + K^2V^2}\delta V + \left(\frac{RT_o}{2RT_o + K^2V^2}\frac{1}{p_o} - \frac{1}{2q_c}\right)V\delta q_c' \qquad (A7)$$

For the speed range for which the trailing anemometer was designed (less than 200 knots)

$$\frac{RT_o}{2RT_o + K^2V^2} \approx \frac{1}{2}$$

Equation (A7) can then be further simplified to

$$\delta(\Delta V_c) = \frac{V}{2}\frac{\delta p'}{p_o} + \delta V + \left(\frac{1}{p_o} - \frac{1}{q_c}\right)\frac{V}{2}\delta q_c'$$

Equation (A7) was used to determine the errors in airspeed for the random data system errors of the variables in tables I and IV. The airspeed error due to temperature measurement was negligible. The sample airspeed errors in table I were computed at the upper and lower calibration limits for each airplane. In table IV, a single sample airspeed was used.

Individual airspeed errors were also combined to give root-mean-square overall system calibration errors at each sample speed for each airplane. The relation used was

$$\text{Combined rms data system error} = \Big[(\text{Error from } \delta p')^2 + (\text{Error from } \delta V)^2 + (\text{Error from } \delta q_c')^2 + (\text{Error from } \delta T')^2\Big]^{1/2} \Big/ \sqrt{4}$$

APPENDIX

Tower Flyby Method

The three airplane measurements used in the tower flyby technique are p', q_c', and T'. The three ground-based measurements which are used are p_1, T_1, and Z_a. The random data system errors in temperature T' and T_1 are negligible and are not included in this treatment. (See trailing anemometer section of this appendix.)

By use of the symbol δ to represent random errors (measured and calculated), the actual values used in the determination of static-pressure position error Δp are

Measured static pressure = $p' + \delta p'$

Measured impact pressure = $q_c' + \delta q_c'$

Measured total temperature = $T' + \delta T' \approx T'$ or Free-air temperature = T'

Measured local static pressure = $p_1 + \delta p_1$

Measured local static temperature = $T_1 + \delta T_1 \approx T_1$

Measured aircraft geometric altitude = $Z_a + \delta Z_a$

The static pressure at the height of the airplane is calculated by a pressure lapse rate of the form

$$p = p_1 \exp\left(\frac{-g\,\Delta Z}{RT_1}\right) = p_1 \exp\left[\frac{-g(Z_a - Z_1)}{RT_1}\right] \tag{A8}$$

where ΔZ is the difference in height between the airplane Z_a and the nearest barometer Z_1.

When random data system errors in p_1 and Z_a are included in the static-pressure relation, equation (A8) becomes

$$p + \delta p = (p_1 + \delta p_1) \exp\left[\frac{-g(Z_a + \delta Z_a - Z_1)}{RT_1}\right]$$

or

$$p + \delta p = (p_1 + \delta p_1) \exp\left[\frac{g(Z_1 - Z_a)}{RT_1}\right] \exp\left(\frac{-g\delta Z_a}{RT_1}\right)$$

or

$$p + \delta p = \left\{ p_1 \exp\left[\frac{g(Z_1 - Z_a)}{RT_1}\right] + \delta p_1 \exp\left[\frac{g(Z_1 - Z_a)}{RT_1}\right] \right\} \exp\left[\frac{-g\delta Z_a}{RT'}\right]$$

By using a series expansion,

$$\exp\left(\frac{-g\delta Z_a}{RT_1}\right) = 1 + \frac{-g\delta Z_a}{RT_1} + \frac{1}{2}\left(\frac{-g\delta Z_a}{RT_1}\right)^{2 \to 0} + \ldots$$

By using this series expansion and letting

$$B = \exp\left[\frac{g(Z_1 - Z_a)}{RT_1}\right] \tag{A9}$$

the equation for $p + \delta p$ becomes

$$p + \delta p = \left[p_1 B + \delta p_1 B\right]\left[1 - \frac{g\delta Z_a}{RT_1}\right]$$

or

$$p + \delta p = p_1 B - p_1 B \frac{g\delta Z_a}{RT_1} + \delta p_1 B - \frac{\delta p_1 B \delta Z_a g}{RT_1}^{\to 0}$$

But from equations (A8) and (A9), $p = Bp_1$; therefore,

$$p + \delta p = p + B\left(-p_1 g \frac{\delta Z_a}{RT_1} + \delta p_1\right)$$

Static-pressure position error Δp is computed as the difference between measured static pressure and the true static pressure:

$$\Delta p = p' - p$$

which becomes

$$\Delta p + \delta(\Delta p) = (p' + \delta p') - (p + \delta p)$$

or

$$\Delta p + \delta(\Delta p) = p' + \delta p' - p - B\left(-p_1 g \frac{\delta Z_a}{RT_1} + \delta p_1\right)$$

when random data system errors are included.

Impact pressure q_c is computed from measured impact pressure and static-pressure position error by the relation

$$q_c = q_c' + \Delta p$$

which becomes

$$q_c + \delta q_c = q_c' + \delta q_c' + \left[\Delta p + \delta(\Delta p)\right]$$

or

$$q_c + \delta q_c = q_c' + \delta q_c' + p' + \delta p' - p - B\left(-p_1 g \frac{\delta Z_a}{RT_1} + \delta p_1\right)$$

when random data system errors are included.

By using the relations for q_c and Δp, the relation for $q_c + \delta q_c$ can be written

$$q_c + \delta q_c = q_c + \delta q_c' + \delta p' + B\left(p_1 g \frac{\delta Z_a}{RT_1} - \delta p_1\right) \tag{A10}$$

Calibrated airspeed is computed by the equation

$$V_c = \frac{1}{K}\sqrt{\frac{2q_c}{\rho_o}}$$

which, with random data system errors in q_c, becomes

$$V_c + \delta V_c = \frac{1}{K}\sqrt{\frac{2(q_c + \delta q_c)}{\rho_o}}$$

The expansion of this equation parallels the expansion of the equation for V_i in the trailing anemometer method except that the random error component of equation (A10) consists of four terms rather than a single term, and q_c is used rather than q_c'. The resulting expansion is analogous to equation (A5):

$$V_c + \delta V_c = V_c\left[1 + \frac{1}{2q_c}\left(\delta q_c' + \delta p' + Bp_1 g\,\frac{\delta Z_a}{RT_1} - B\delta p_1\right)\right] \tag{A11}$$

As in the trailing anemometer method, V_i is computed from

$$V_i = \frac{1}{K}\sqrt{\frac{2q_c'}{\rho_o}}$$

and incorporating random data system error is given by equation (A5) as

$$V_i + \delta V_i = V_i\left(1 + \frac{\delta q_c'}{2q_c'}\right)$$

The airspeed position error in terms of airspeed is

$$\Delta V_c = V_c - V_i$$

which actually contains random data system errors so that

$$\Delta V_c + \delta(\Delta V_c) = V_c + \delta V_c - (V_i + \delta V_i)$$

or by substituting from equations (A11) and (A5),

$$\Delta V_c + \delta(\Delta V_c) = V_c\left[1 + \frac{1}{2q_c}\left(\delta q_c' + \delta p' + Bp_1 g\,\frac{\delta Z_a}{RT_1} - B\delta p_1\right)\right] - V_i\left(1 + \frac{\delta q_c'}{2q_c'}\right)$$

By substituting for B from equation (A9) and grouping terms, the general expression for random data system errors in terms of airspeed becomes

$$\delta(\Delta V_c) = \delta q_c'\left(\frac{V_c}{2q_c} - \frac{V_i}{2q_c'}\right) + \frac{V_c}{2q_c}\,\delta p' + \frac{V_c p_1}{2q_c}\exp\left[\frac{g(Z_1 - Z_a)}{RT_1}\right]\frac{g\delta Z_a}{RT_1}$$

$$- \frac{V_c}{2q_c}\exp\left[\frac{g(Z_1 - Z_a)}{RT_1}\right]\delta p_1 \tag{A12}$$

Tables II and IV present examples of airspeed errors caused by random data system errors. Several assumptions were made in computing these errors from equation (A12). First, to isolate the effects of random data system errors, it

was assumed that there was zero static-pressure position error $\Delta p = 0$. This meant that

$$q_c' = q_c$$

and

$$V_c = V_i$$

As a result, the $\delta q_c'$ term does not contribute to the random error.

The geometry from the tower flyby arrangement in figure 6 was used to assume values of g, Z, T_1, p_1, and $Z_1 - Z_a$ for the sample solutions. The elevation at the lowest station on the measurement tower was assumed for Z_1 (Z_1 = 45.7 m (150 ft)), and the values of static temperature and static pressure corresponding to that altitude in the standard atmosphere were used for T_1 and p_1, respectively. A value of g corresponding to Z_1 was also used. A value of $Z_1 - Z_a$ = 7.65 m (25 ft) was assumed as this is one-half the distance between the first and second or second and third measurement stations.

Table II presents airspeed errors computed for airplane C at the upper and lower calibration limits for the tower flyby runs. Table IV presents a single-sample airspeed for direct comparison with the trailing anemometer method.

Individual airspeed errors were also combined to give root-mean-square overall system calibration errors at each sample speed in tables II and IV. The relation was:

$$\text{Combined rms data system error} = \frac{1}{\sqrt{5}}\Big[(\text{Error from } \delta p')^2 + (\text{Error from } \delta Z_a)^2 + (\text{Error from } \delta p_1)^2 + (\text{Error from } \delta T')^2 + (\text{Error from } \delta T_1)^2\Big]^{1/2}$$

where the the errors from $\delta T'$ and δT_1 were negligible.

REFERENCES

1. Fisher, Bruce D.; Stough, H. Paul; and Kershner, David D.: Trailing Anemometer for Low Airspeed Calibration. [Preprint] 760461, Soc. Automot. Eng., Apr. 1976.

2. Kershner, David D.: A Suspended Anemometer System for Measuring True Airspeed on Low-Speed Airplanes. NASA TN D-8523, 1977.

3. Richardson, Norman R.; and Pearson, Albin O.: Wind-Tunnel Calibrations of a Combined Pitot-Static Tube, Vane-Type Flow-Direction Transmitter and Stagnation Temperature Element at Mach Numbers From 0.60 to 2.87. NASA TN D-122, 1959.

4. Mechtly, E. A.: The International System of Units - Physical Constants and Conversion Factors (Second Revision). NASA SP-7012, 1973.

5. Gracey, William: Measurement of Static Pressure on Aircraft. NACA Rep. 1364, 1958. (Supersedes NACA TN 4184.)

6. Gracey, William; and Scheithauer, Elwood F.: Flight Investigation of the Variation of Static-Pressure Error of a Static-Pressure Tube With Distance Ahead of a Wing and a Fuselage. NACA TN 2311, 1951.

7. Holmes, Bruce J.: Flight Evaluation of an Advanced Technology Light Twin-Engine Airplane (ATLIT). NASA CR-2832, 1977.

8. Thompson, Floyd L.: The Measurement of Air Speed of Airplanes. NACA TN 616, 1937.

9. Aiken, William S., Jr.: Standard Nomenclature for Airspeeds With Tables and Charts for Use in Calculation of Airspeed. NACA Rep. 837, 1946. (Supersedes NACA TN 1120.)

10. Gracey, William: Position Errors of the Service Airspeed Installations of 10 Airplanes. NACA TN 1892, 1949.

TABLE I.- AIRCRAFT INSTRUMENTATION SYSTEM RANGES AND RANDOM DATA SYSTEM ERRORS FOR THE TRAILING ANEMOMETER METHOD

(a) Airplane A

Variable	Range	Random data system errors	Airspeed errors based on random data system errors for standard sea-level conditions, knots	
			V = 40 knots	V = 100 knots
p'	101.4 to 84.3 kPa (2115.8 to 1761.12 lb/ft^2)	$\delta p' = \pm 170.5$ Pa (± 3.56 lb/ft^2)	≈0	≈0
q_c'	0 to 1.4 kPa (0.0 to 28.8 lb/ft^2)	$\delta q_c' = \pm 14$ Pa (± 0.288 lb/ft^2)	± 1.06	± 0.42
T'	247 to 306 K (445° to 550° R)	$\delta T' = \pm 0.6$ K (± 1.0° R)	0	0
V	26.1 to 130.4 knots (30.0 to 150.0 mi/hr	$\delta V = \pm 1$ knot (± 1.2 mi/hr)	± 1.0	± 1.02
α	-10° to 30°	± 0.4°	Not applicable	Not applicable
		Combined rms data system error	± 0.54	± 0.53

TABLE I.- Continued

(b) Airplane B

Variable	Range	Random data system errors	Airspeed errors based on random data system errors for standard sea-level conditions, knots	
			V = 60 knots	V = 110 knots
p'	101.4 to 69.6 kPa (2116.8 to 1452.96 lb/ft^2)	$\delta p' = \pm 630$ Pa (± 13.25 lb/ft^2)	± 0.19	± 0.34
q_c'	0 to 2.1 kPa (0.0 to 43.2 lb/ft^2)	$\delta q_c' = \pm 40$ Pa (± 0.864 lb/ft^2)	± 2.11	± 1.12
T'	228 to 311 K (410° to 560° R)	$\delta T' = \pm 1.7$ K (± 3.0° R)	≈ 0	≈ 0
V	0 to 149 knots	$\delta V = \pm 3$ knots	± 2.98	± 2.94
α	-5.9° to 14.4°	± 0.4°	Not applicable	Not applicable
		Combined rms data system error	± 1.83	± 1.61

TABLE I.- Concluded

(c) Airplane C

Variable	Range	Random data system errors	Airspeed errors based on random data system errors for standard sea-level conditions, knots	
			V = 50 knots	V = 140 knots
p'	103.4 to 0 kPa (2169 to 0 lb/ft^2)	$\delta p' = \pm 2070$ Pa (± 43.2 lb/ft^2)	± 0.51	± 1.38
q_c'	0 to 6.9 kPa (0 to 144 lb/ft^2)	$\delta q_c' = \pm 100$ Pa (± 2 lb/ft^2)	± 5.88	± 2.02
T'	255 to 311 K (460° to 560° R)	$\delta T' = \pm 0.6$ K (± 1.0° R)	0	0
V	0 to 142.6 knots	$\delta V = \pm 1.1$ knots	± 1.1	± 1.1
α	± 20°	± 0.4°	Not applicable	Not applicable
		Combined rms data system error	± 3.0	± 1.34

TABLE II.- AIRCRAFT AND GROUND-BASED INSTRUMENTATION RANGES AND RANDOM DATA SYSTEM ERRORS FOR TOWER FLYBY METHOD FOR AIRPLANE C

Variable	Range	Random data system errors	Airspeed errors based on random data system errors, knots (a)	
			V = 90 knots	V = 170 knots
Airborne				
p'	103.1 to 96.0 kPa (2154.24 to 2004.48 lb/ft^2)	$\delta p' = \pm 170$ Pa (± 3.5 lb/ft^2)	± 5.72	3.0
q_c'	0 to 6.9 kPa (0 to 144 lb/ft^2)	$\delta q_c' = \pm 100$ Pa (± 2 lb/ft^2)	See appendix	See appendix
T'	255 to 311 K (460° to 560° R)	$\delta T' = \pm 0.6$ K (± 1.0° R)	0	0
α	± 20°	± 0.40°	Not applicable	Not applicable
Ground based				
Z_a	Not applicable	$\delta Z_a = \pm 0.2$ m (0.35 lb/ft^2)	≈ 0	≈ 0
p_1	100 to 104k Pa (2086.45 to 2192.54 lb/ft^2) 29.5 to 31 in Hg	$\delta p_1 = \pm 17$ Pa (0.35 lb/ft^2)	± 0.6	± 0.3
T_1	244 to 300 K (440° to 540° R)	$\delta T_1 = \pm 0.6$ K (± 1.0° R)	≈ 0	≈ 0
		Combined rms data system error	± 2.6	± 1.3

[a]Assume standard atmosphere; $Z_a = 45.7$ m; $\Delta Z = 7.65$ m. See appendix.

TABLE III.- TEST RUNS

(a) Airplane A

Trailing anemometer method - steady runs
Weight: 45 236 to 44 240 N (10 170 to 9946 lb)
Cable length: 46 m (152 ft)

Run	V_i, knots	Flaps
1 to 5	88.3, 85.25, 81.0, 74.7, 69.7	Up
6 to 15	82.5, 78.3, 74.3, 68.6, 62.2 58.0, 52.7, 49.5, 46.1, 44.0	Down

(b) Airplane B

Trailing anemometer method - Steady runs
Weight: 12 543 to 11 787 N (2820 to 2650 lb)

Run	V_i, knots	Flaps	Cable length, m (ft)	Gear
1 to 6	73.9, 82.6, 91.3, 100, 108.7	Up	30.5 (100)	Up
6 to 11	65.2, 69.6, 73.9, 82.6, 91.3, 100	Down	30.5 (100)	Up
12 to 17	73.9, 82.6, 87.0, 91.3, 100.0, 108.7	Down	15.2 (50)	Up

TABLE III.- Concluded

(c) Airplane C

Trailing anemometer method - steady runs
Weight: 17 570 to 17 348 N (3950 to 3900 lb)
Cable length: 30.5 m (100 ft)

Run	V_i, knots	Flaps	Gear
1 to 3	75, 90, 110	Up	Up

Trailing anemometer method - deceleration runs
Weight: 17 570 to 17 348 N (3950 to 3900 lb)
Cable length: 30.5 m (100 ft)

Run	V_i, knots	Flaps	Gear	Power
1	130 to stall	Up	Up	Bleed-off
2	130 to stall	Up	Up	Off
3	110 to stall	10°	Up	Bleed-off
4	110 to stall	20°	Up	Bleed-off
5	110 to stall	30°	Up	Bleed-off
6	110 to stall	30°	Up	Approach
7	110 to stall	40°	Up	Bleed-off

Tower flyby method
Weight: 17 615 to 17 259 N (3960 to 3880 lb)

Run	V_i, knots	Flaps	Gear
1 to 3	87, 105, 130	Up	Up

TABLE IV.- COMPARISON OF RANDOM DATA SYSTEM ERRORS FOR THE TRAILING ANEMOMETER AND TOWER FLYBY METHODS

Variable	Range	Random data system errors (1-percent full scale)	Effect of sensor/data system random errors on airspeed calibration accuracy at V = 100 knots, knots	
			Trailing anemometer method	Tower flyby method[a]
Airborne				
p	101.4 to 84.3 kPa (2116.8 to 1761.12 lb/ft^2)	$\delta p' = \pm 170.5$ Pa (± 3.56 lb/ft^2)	± 0.08	± 5.23
q_c	0.0 to 1.4 kPa (0.0 to 28.8 lb/ft^2)	$\delta q_c' = \pm 14$ Pa (± 0.288 lb/ft^2)	± 0.42	See appendix
T	247 to 306 K (445° to 550° R)	$\delta T' = \pm 0.6$ K (± 1° R)	0	0
V	26.1 to 130.4 knots	$\delta V = 1$ knot	± 0.98	Not applicable
Ground based				
Z_a	Not applicable	$\delta Z_a = \pm 0.2$ m (± 0.5 ft)[b]	Not applicable	+0.06
p_1	100 to 105 kPa (2086.45 to 2192.54 lb/ft^2)	$\delta p_1 = \pm 50.75$ Pa (± 1.06 lb/ft^2)	Not applicable	± 1.56
T_1	244 to 300 K (440° to 540° R)	$\delta T_1 = \pm 0.6$ K (± 1° R)	Not applicable	0
		Combined rms data system error	± 0.53	± 2.44

[a]Assume: Standard atmosphere; $Z_a = 45.7$ m; $\Delta Z = 7.65$ m. See appendix.
[b]Not a 1-percent full-scale error. Based on radar documentation.

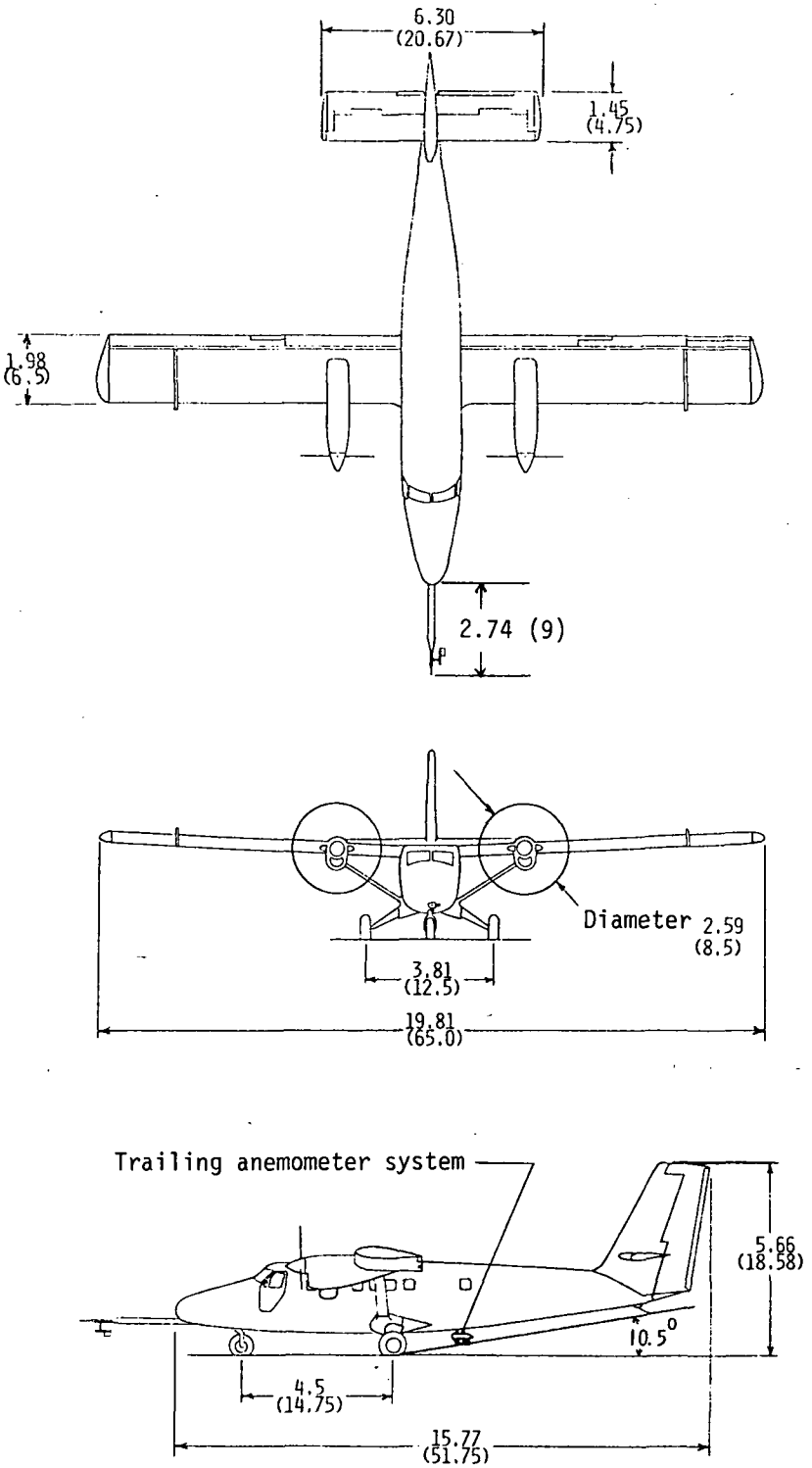

(a) Airplane A.

Figure 1.- Three views of airplanes. All dimensions are in m (ft).

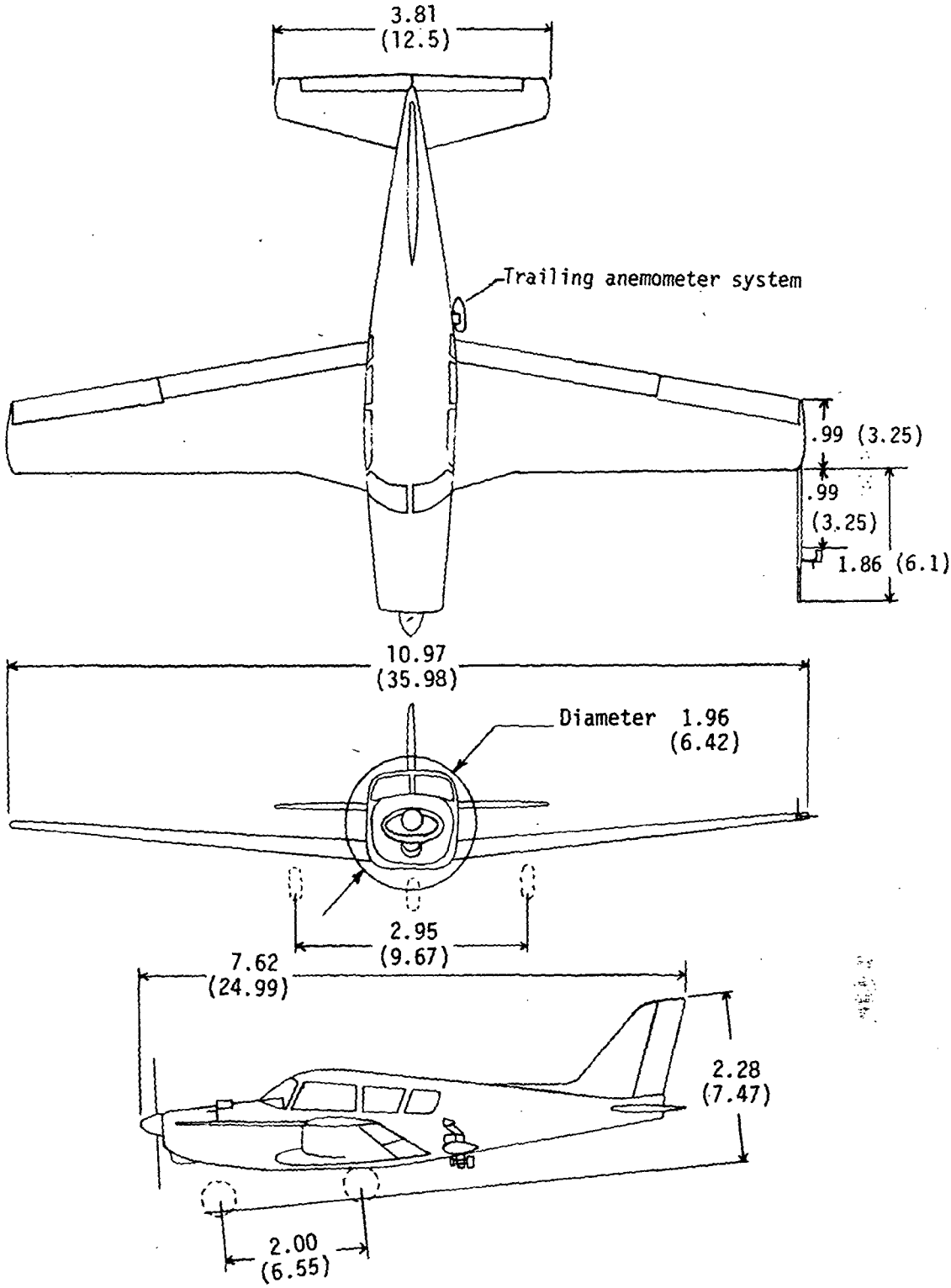

(b) Airplane B.

Figure 1.- Continued.

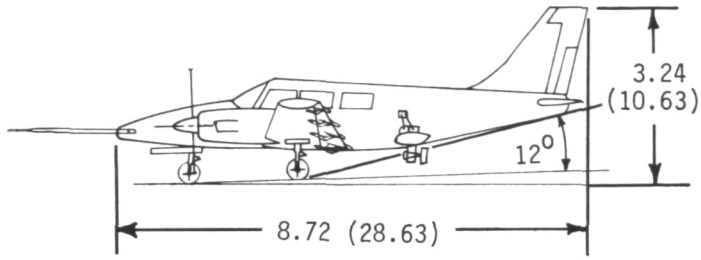

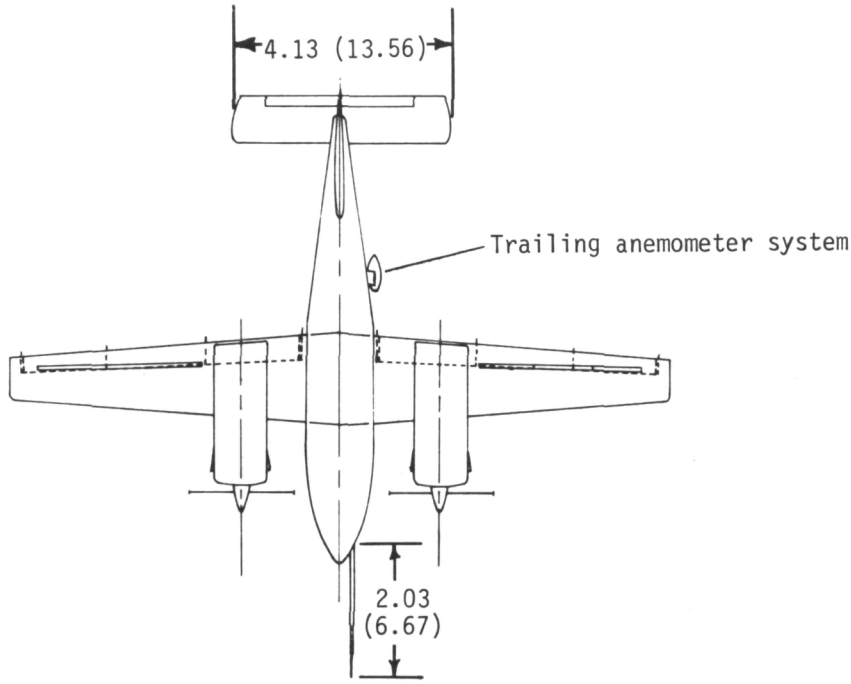

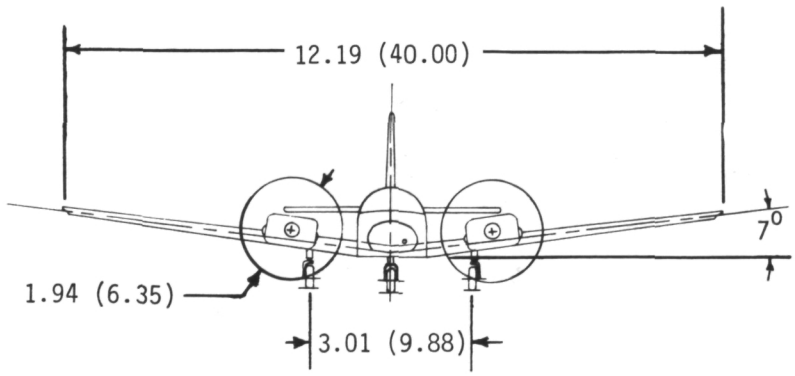

(c) Airplane C.

Figure 1.- Concluded.

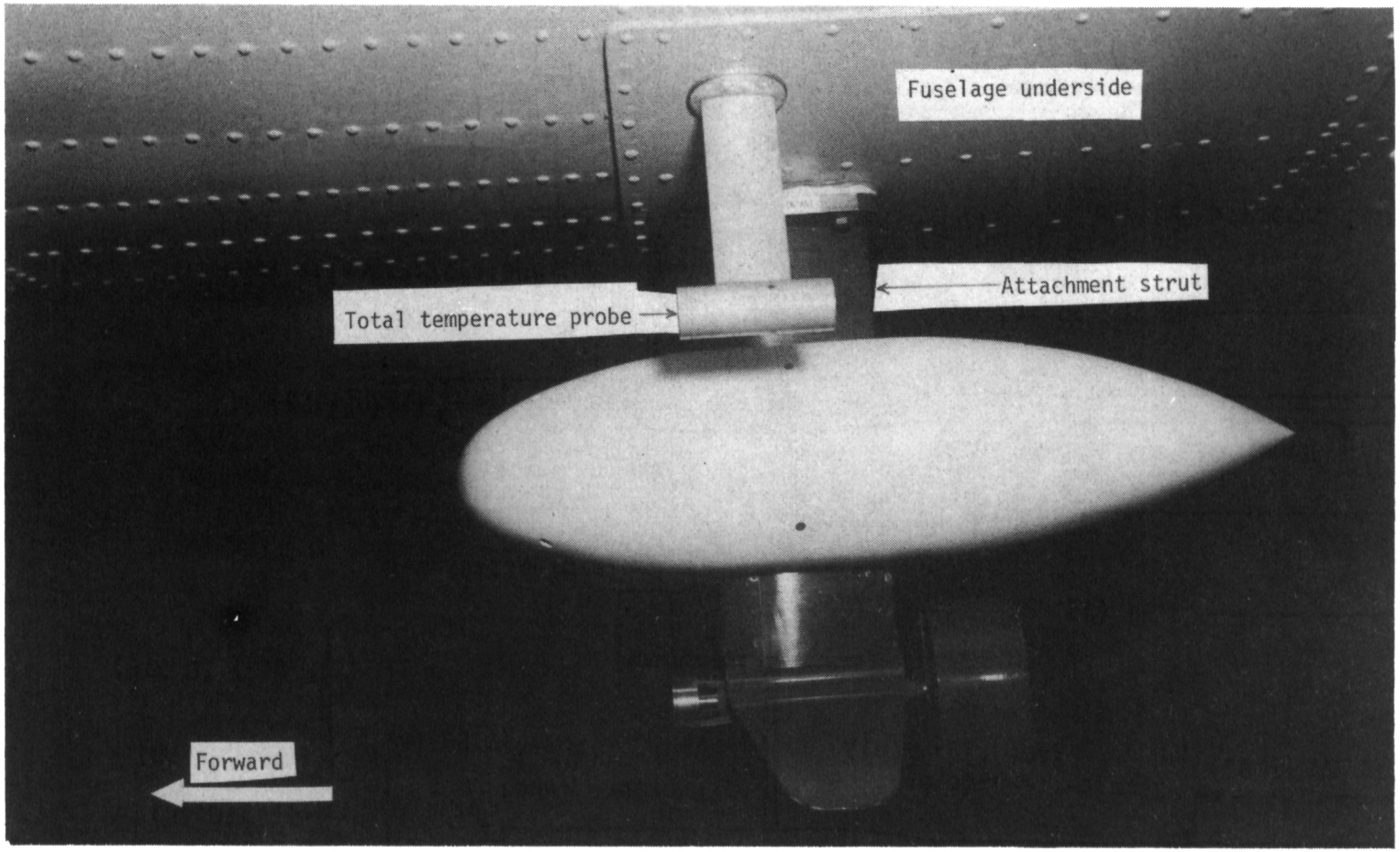

L-74-1258.1

(a) Installation on airplane A.

Figure 2.- Trailing anemometer installations.

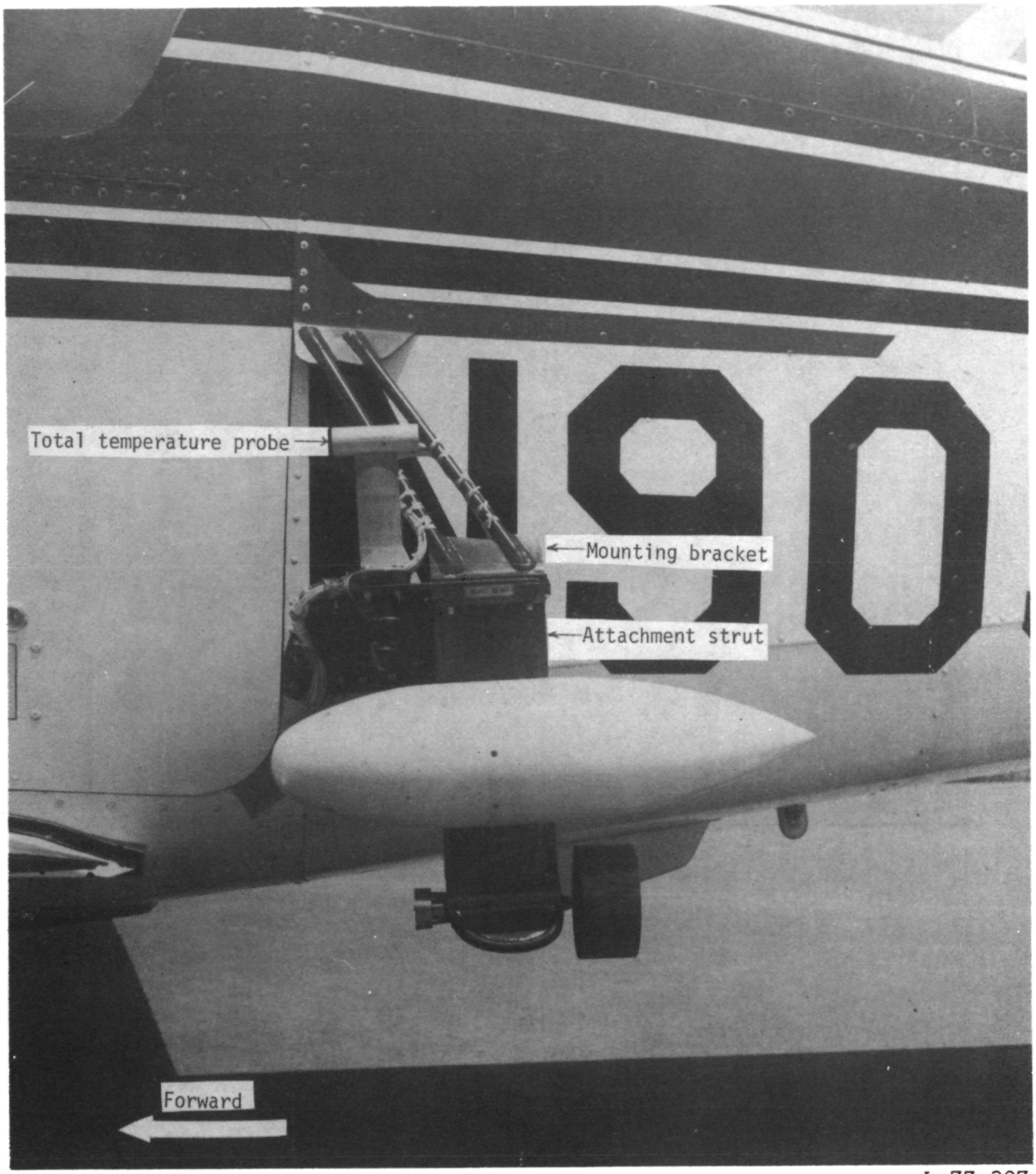

L-77-397

(b) Installation on airplane B.

Figure 2.- Continued.

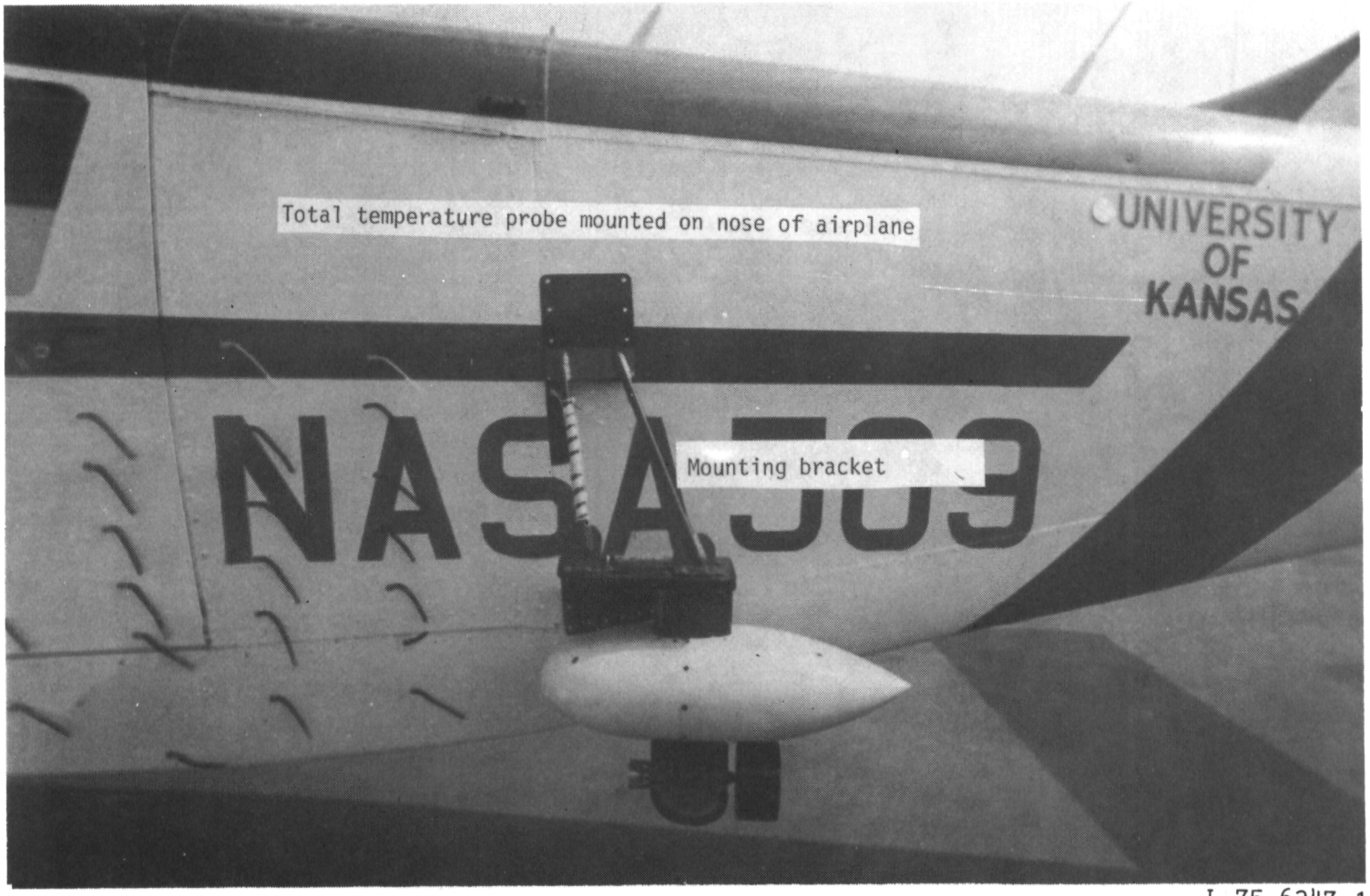

L-75-6347.1

(c) Installation on airplane C.

Figure 2.- Concluded.

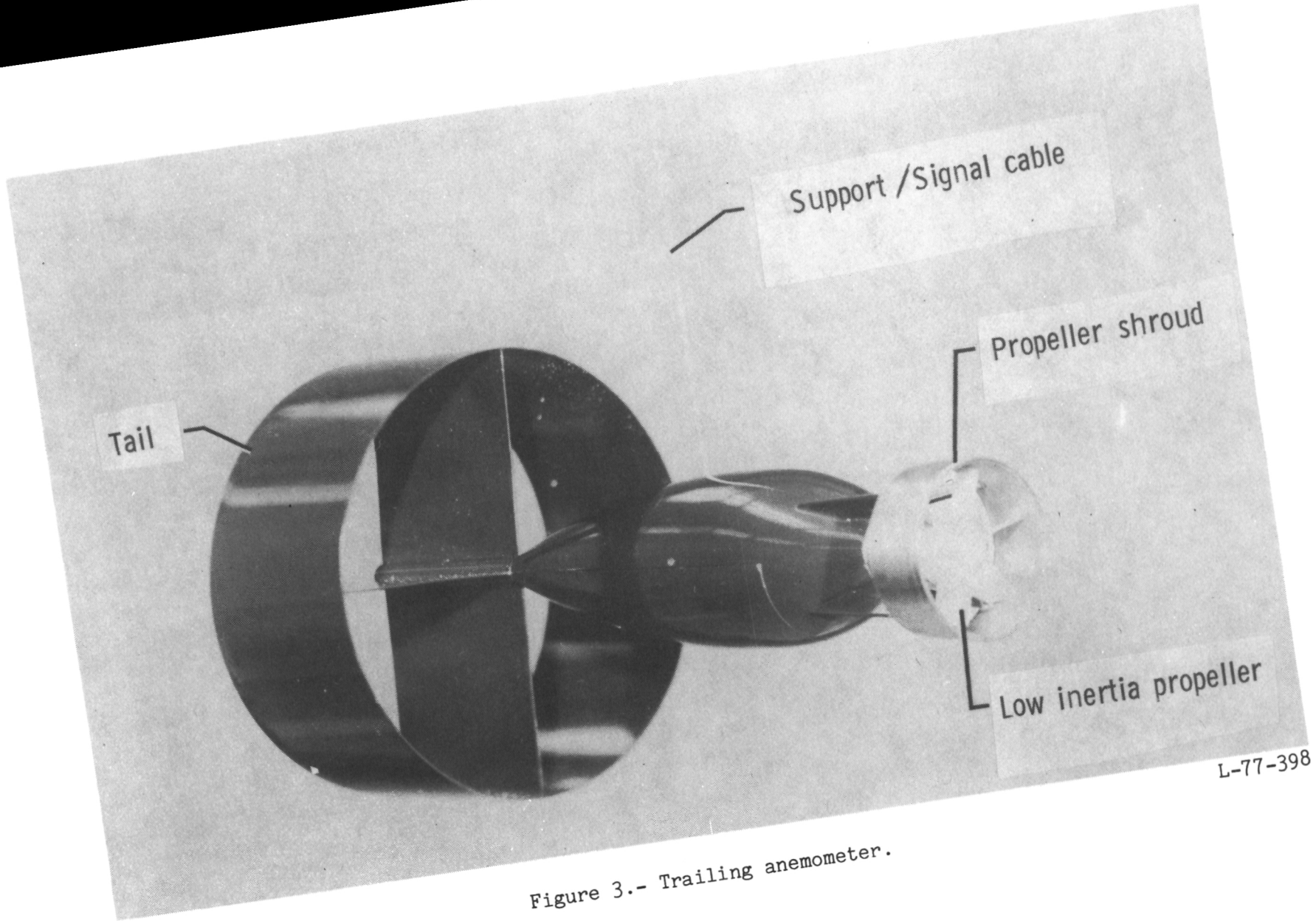

Figure 3.- Trailing anemometer.

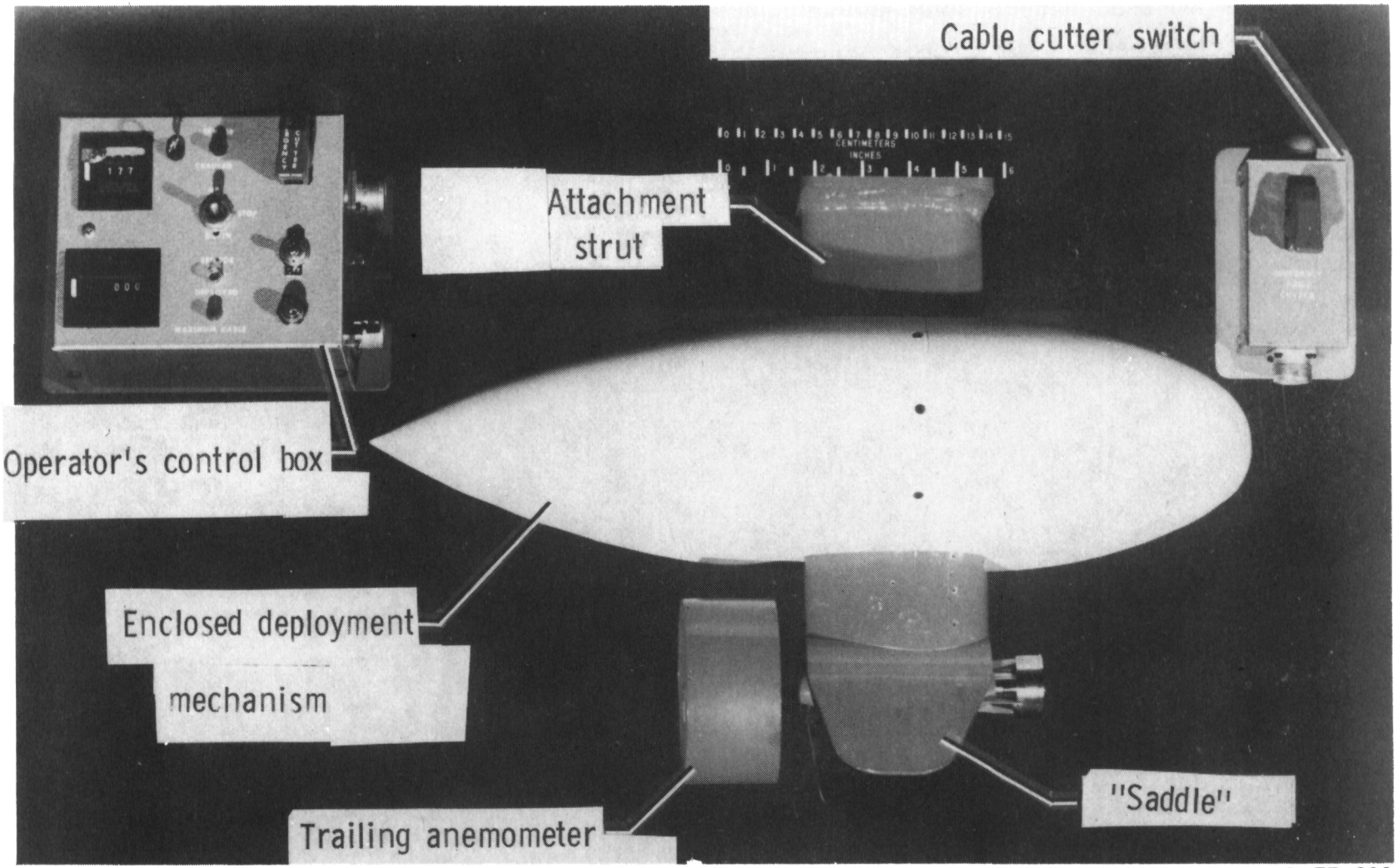

Figure 4.- Trailing anemometer system components.

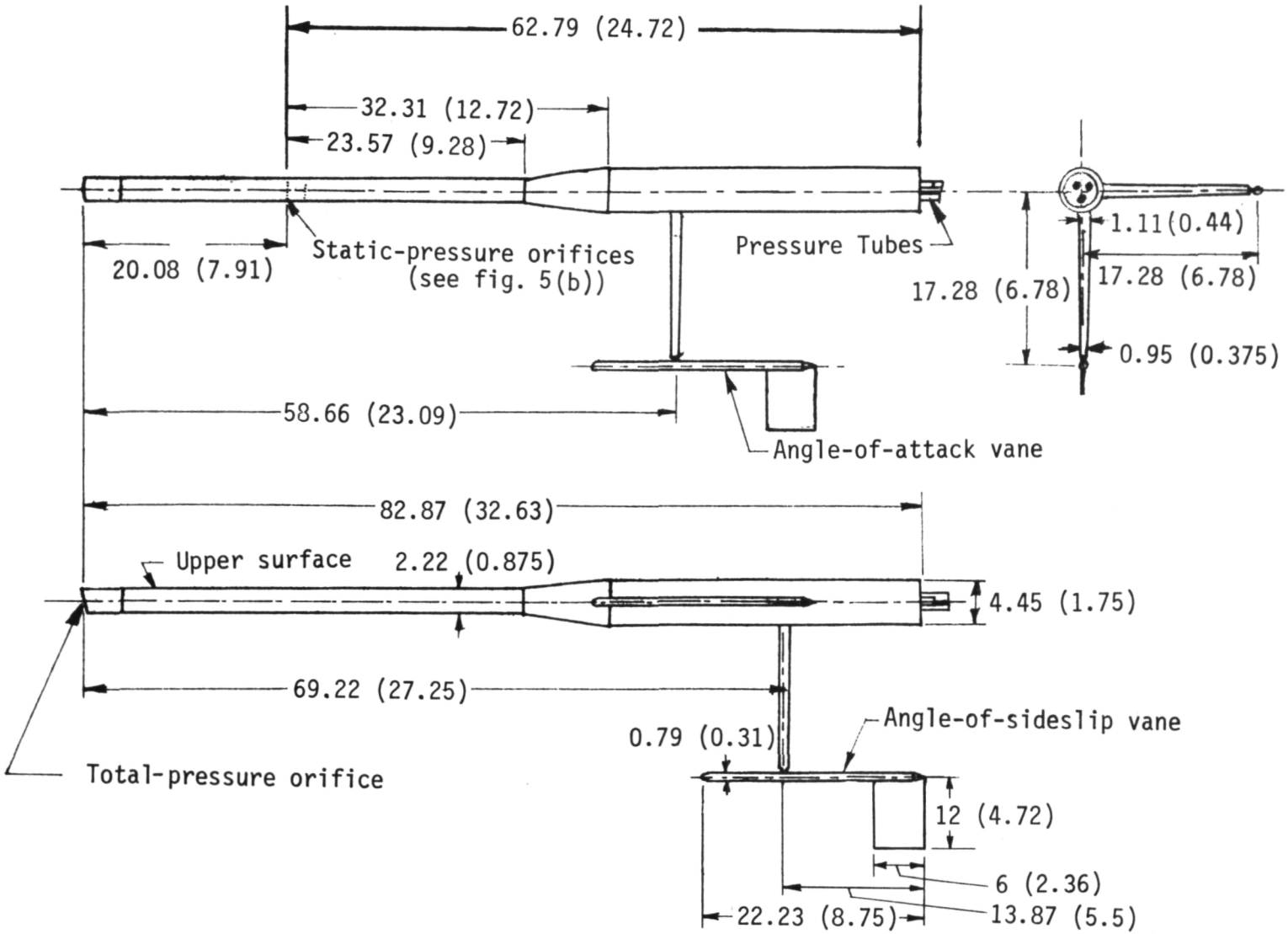

(a) Plan and side views.

Figure 5.- Details of combined pitot-static tube and vane-type flow-direction probe.
All dimensions are in cm (in.).

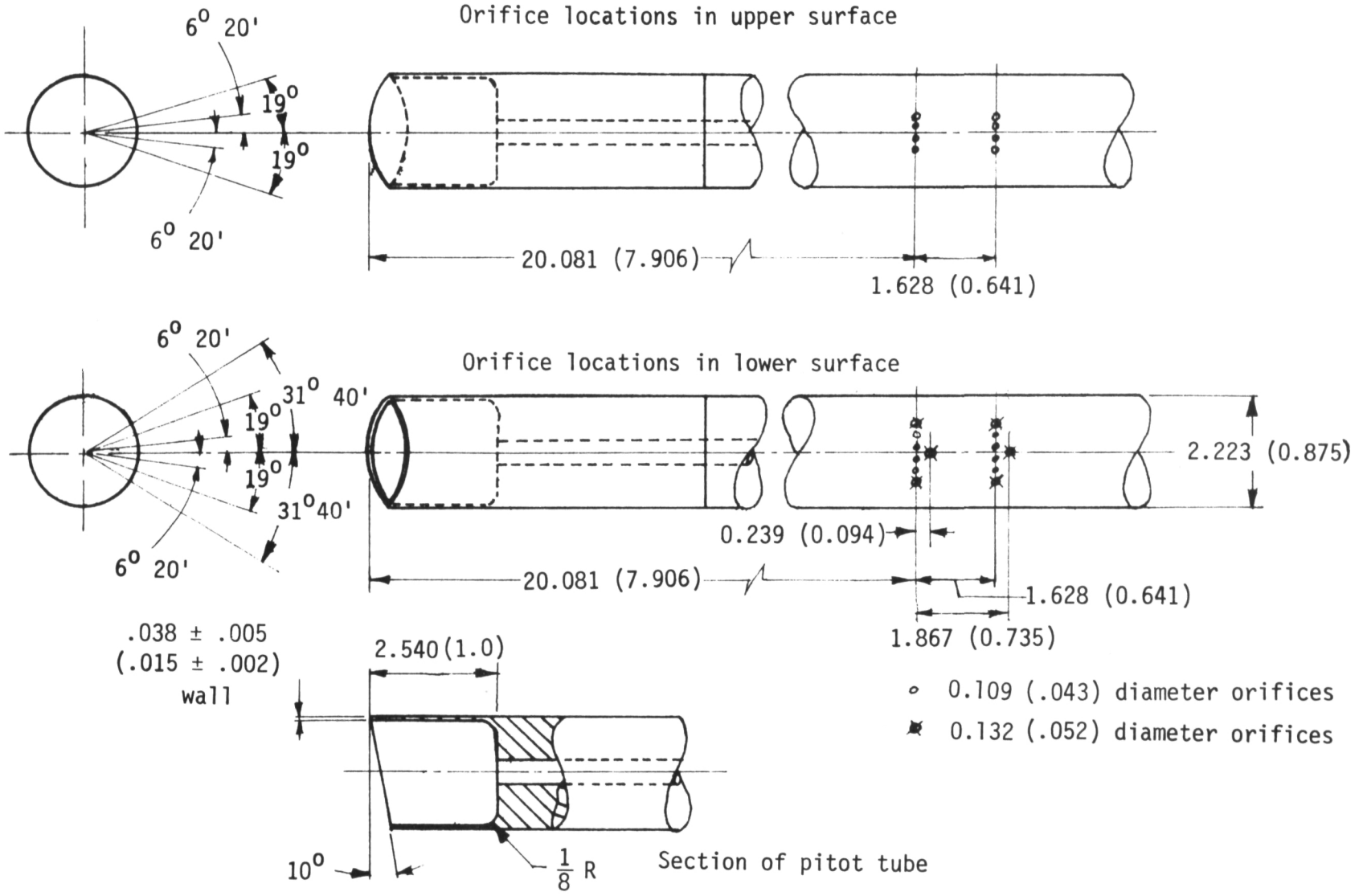

(b) Details of pitot-static tube. All dimensions are in cm (in.).

Figure 5.- Concluded.

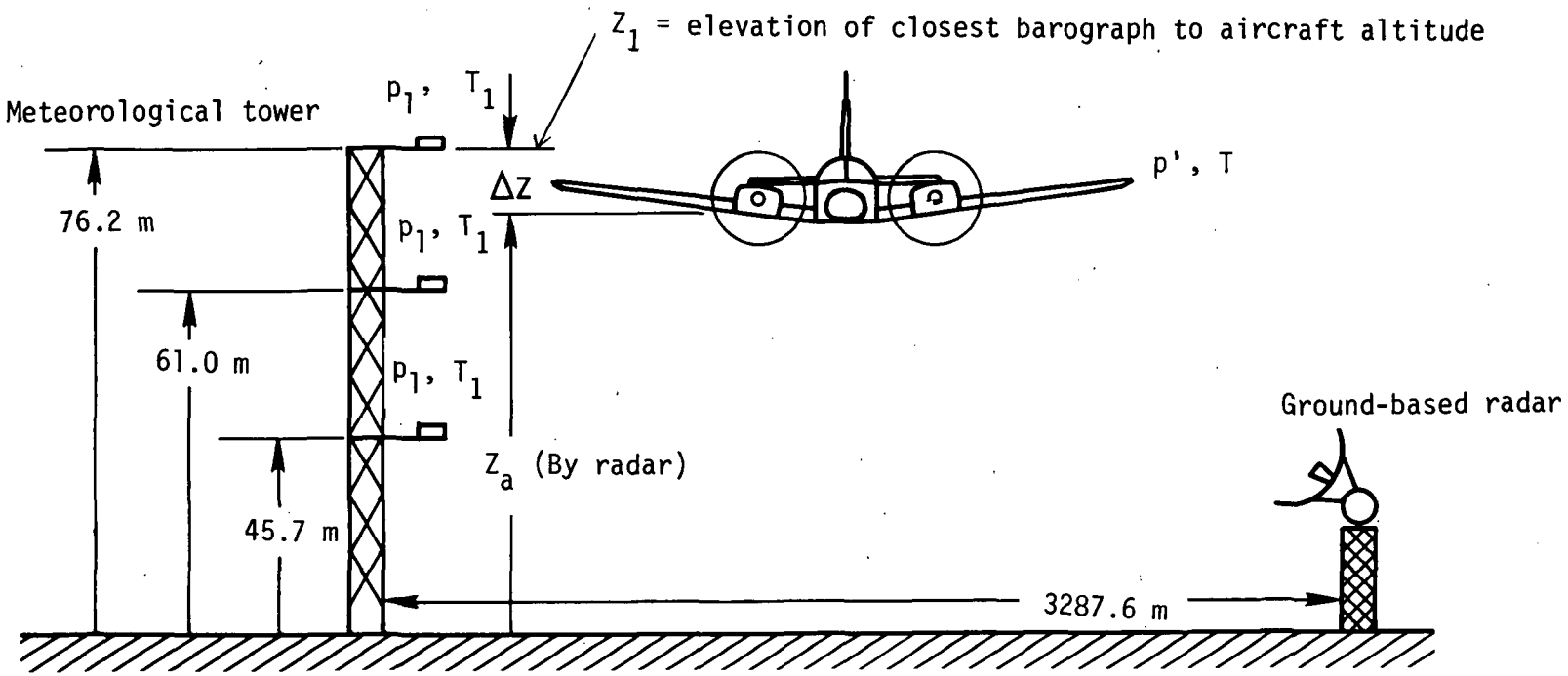

Figure 6.- Schematic of tower flyby equipment.

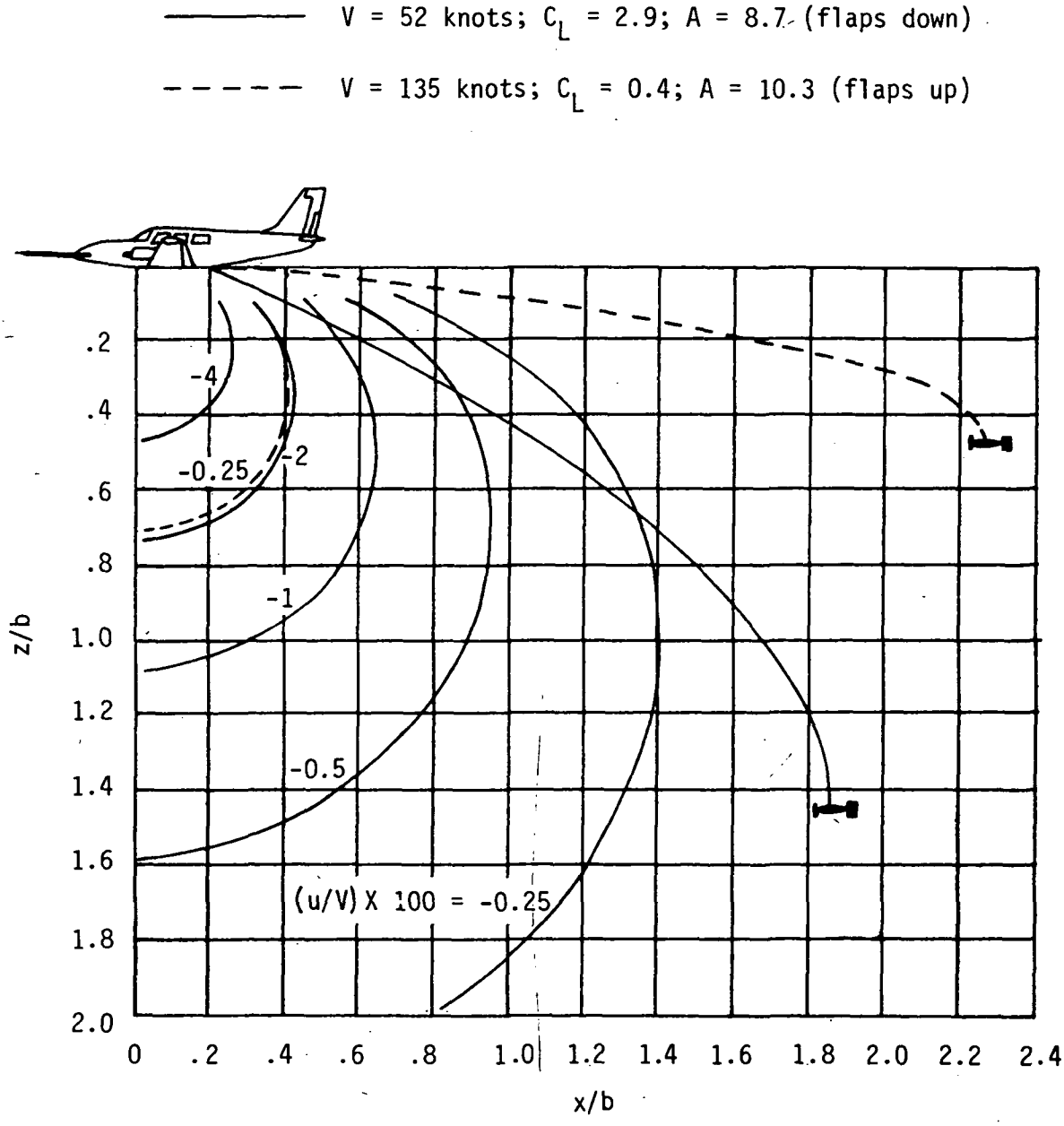

Figure 7.- Induced velocity error and anemometer trail position for two airplane conditions.

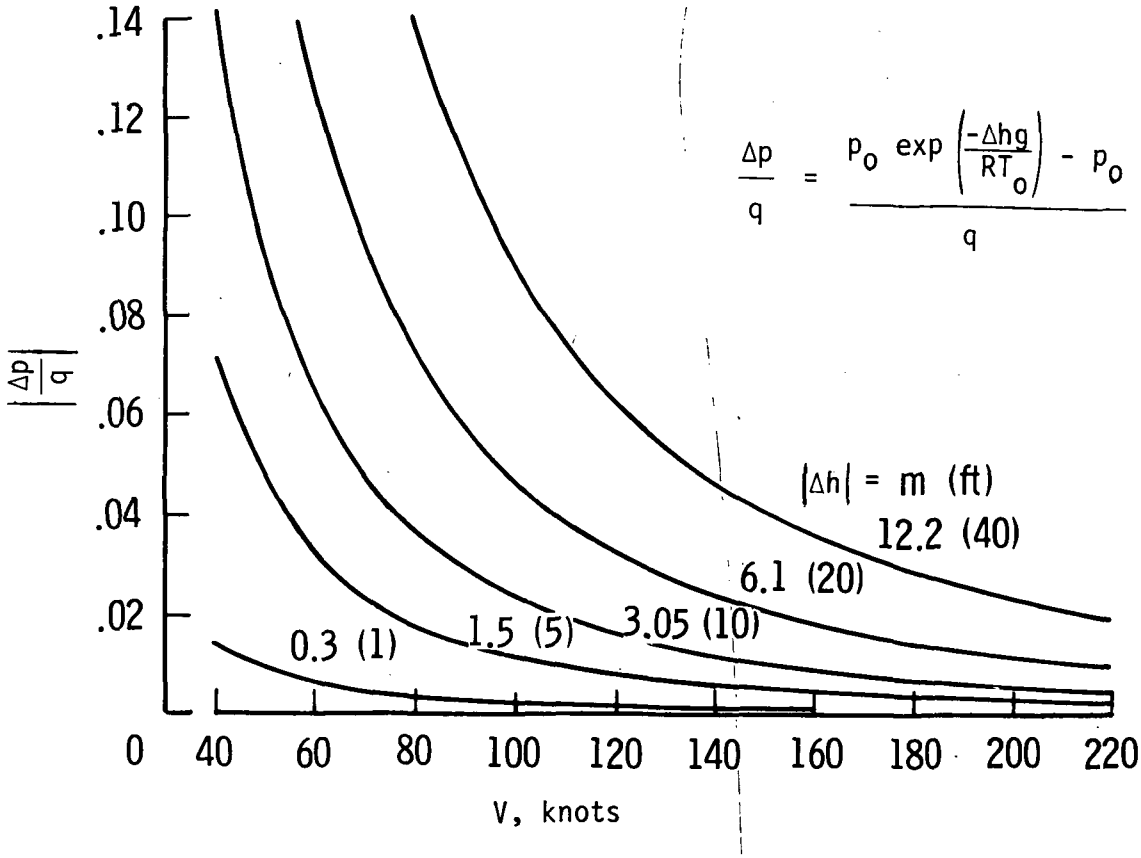

Figure 8.- Effect of altitude error on tower flyby airspeed calibration assuming standard sea-level conditions.

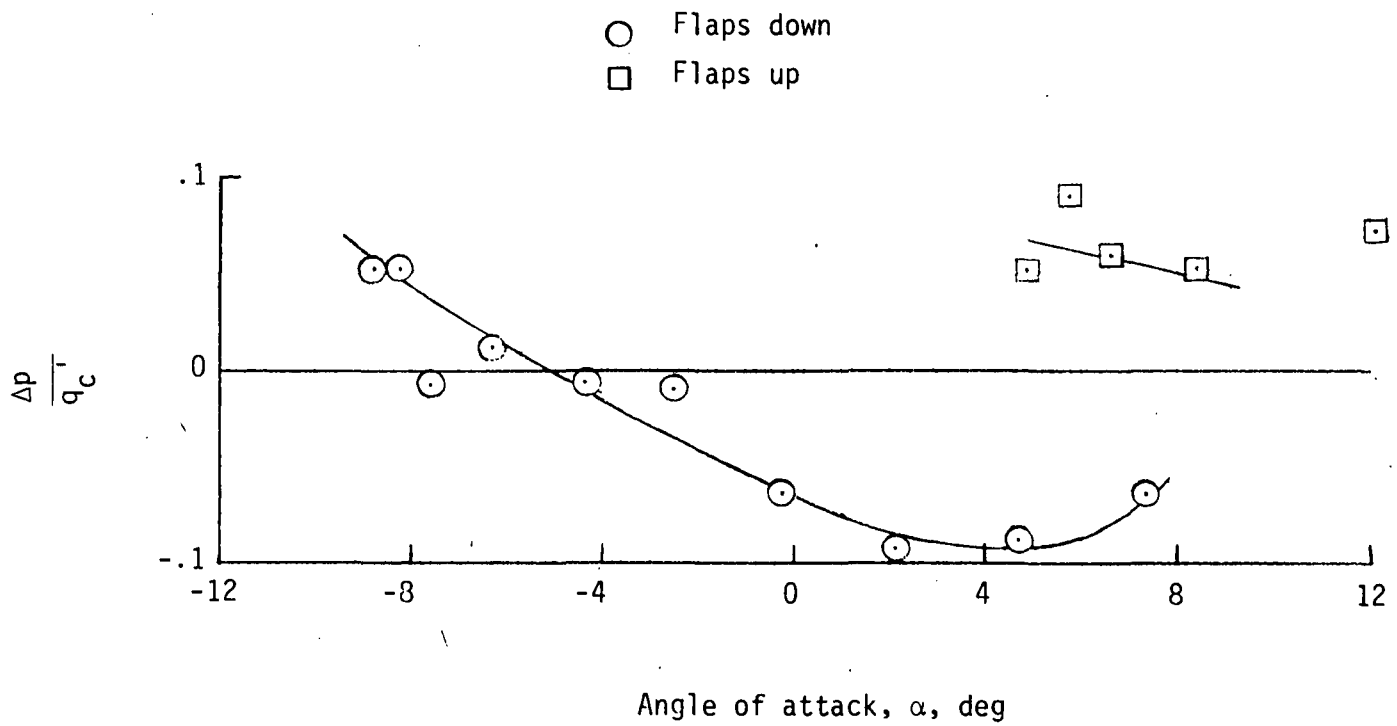

Figure 9.- Variation of static-pressure position error with angle of attack for nose-boom probe of airplane A. Trailing anemometer method - steady runs.

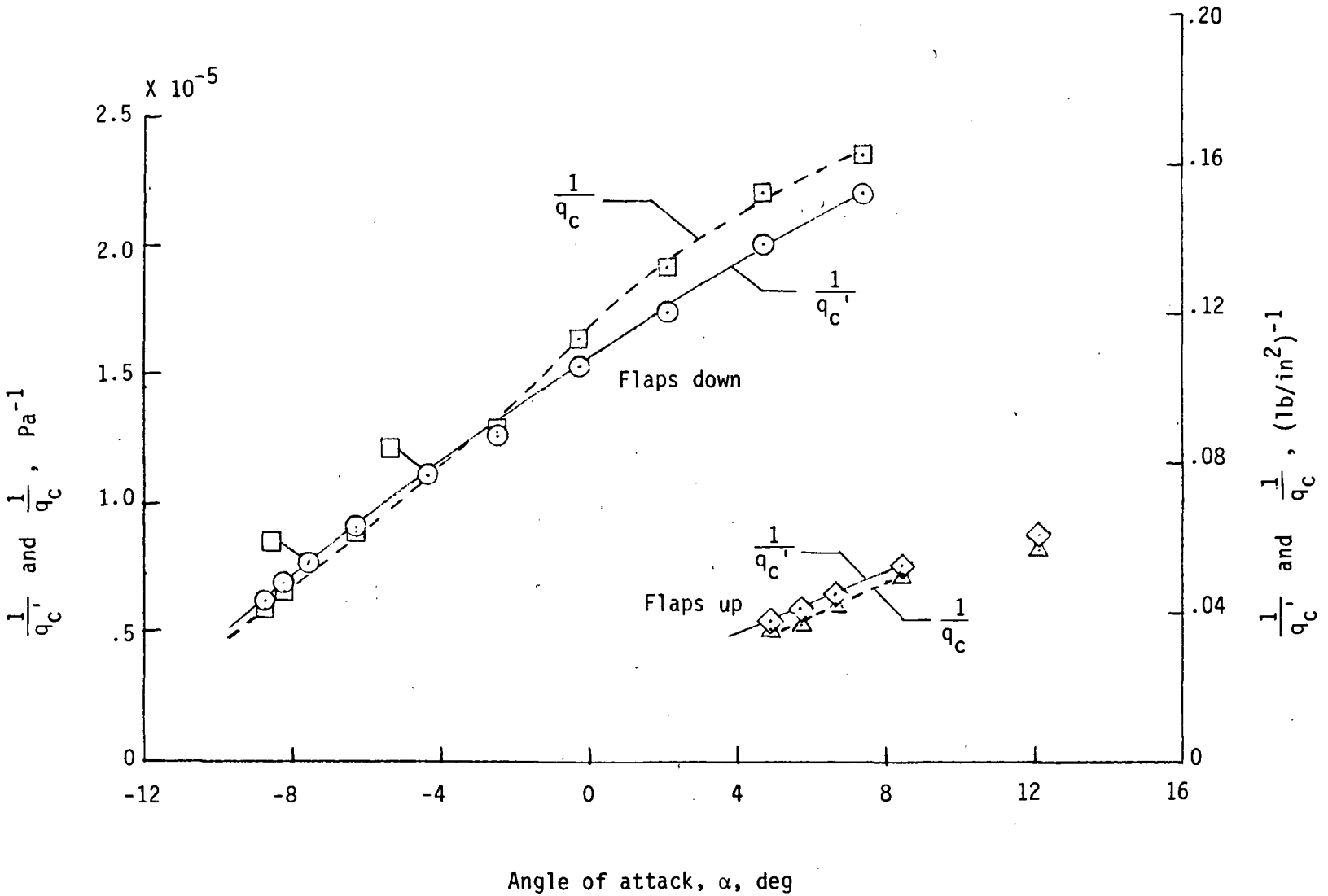

Figure 10.- Variation of impact pressure and measured impact pressure with angle of attack for nose-boom probe of airplane A. Trailing anemometer method - steady runs.

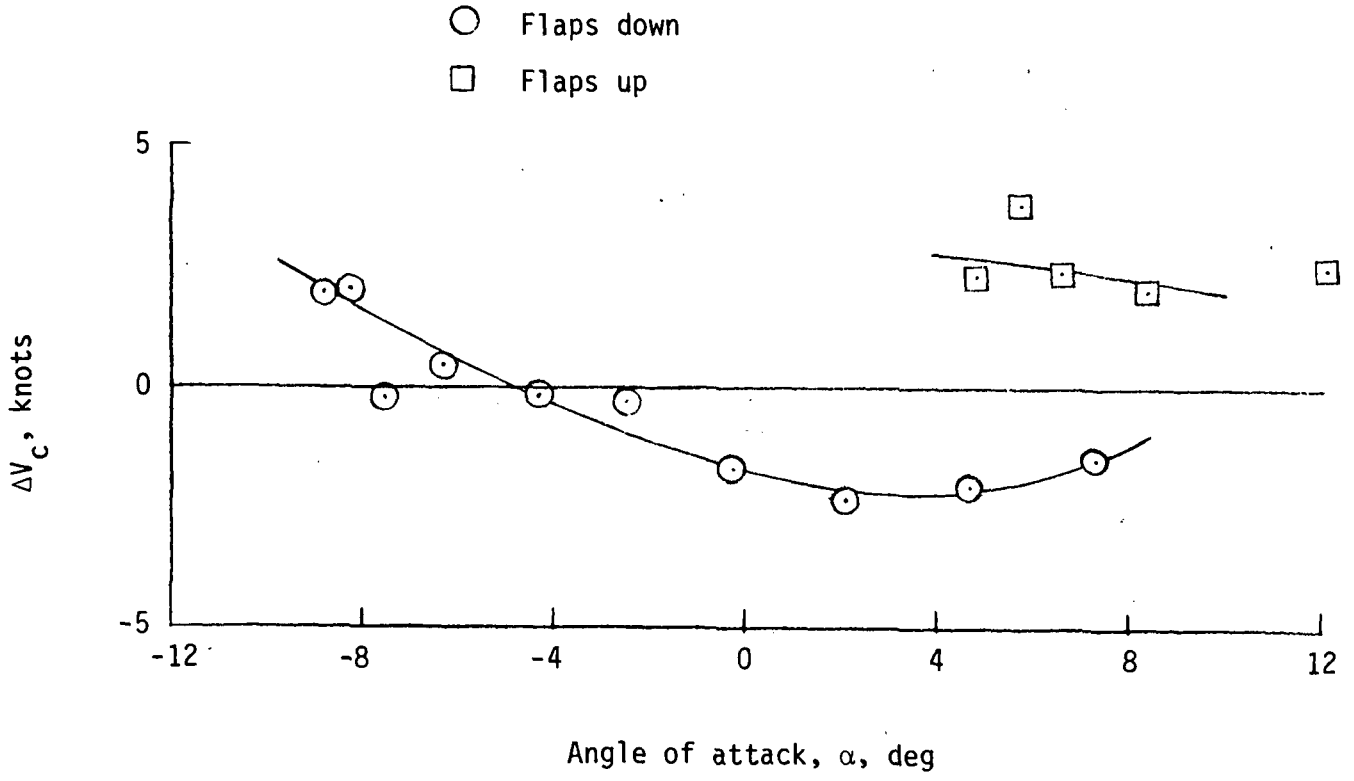

Figure 11.- Variation of airspeed error with angle of attack for nose-boom probe of airplane A. Trailing anemometer method - steady runs.

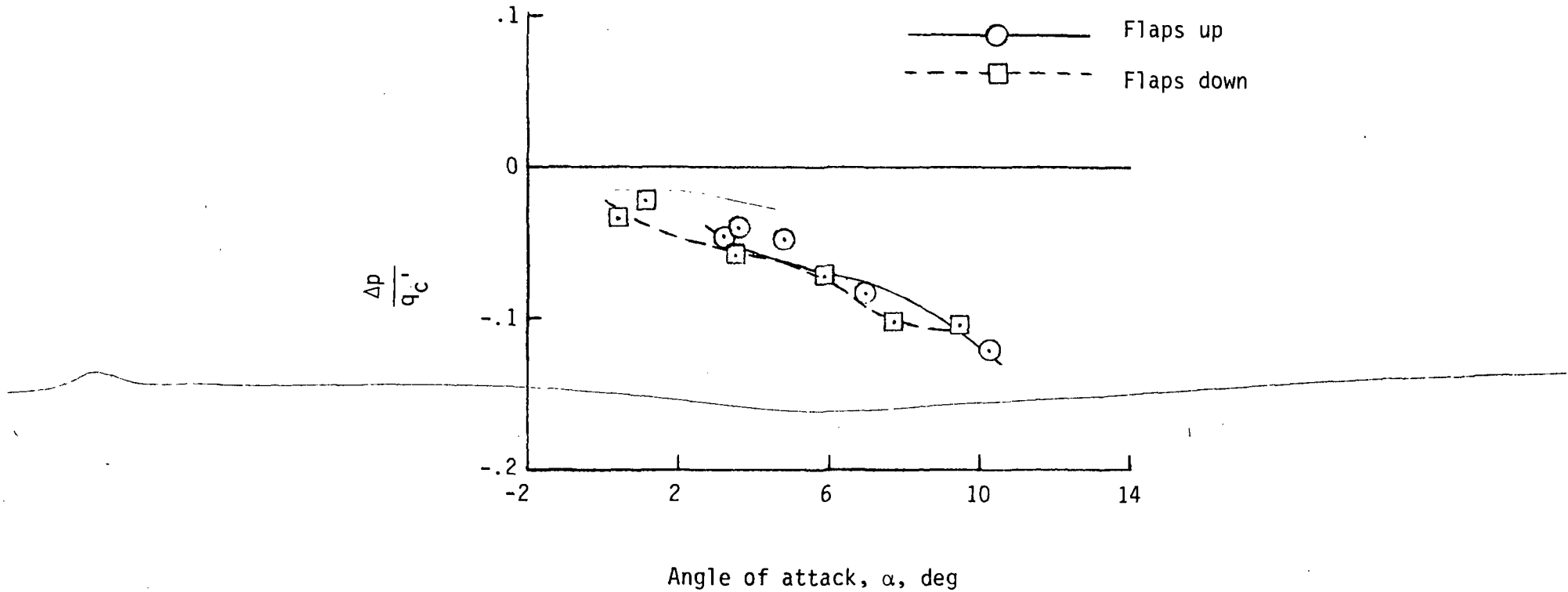

Figure 12.- Variation of static-pressure position error with angle of attack for wing-tip boom probe of airplane B. Trailing anemometer method - steady runs. Cable length, 30.5 m (100 ft) or 2.8b.

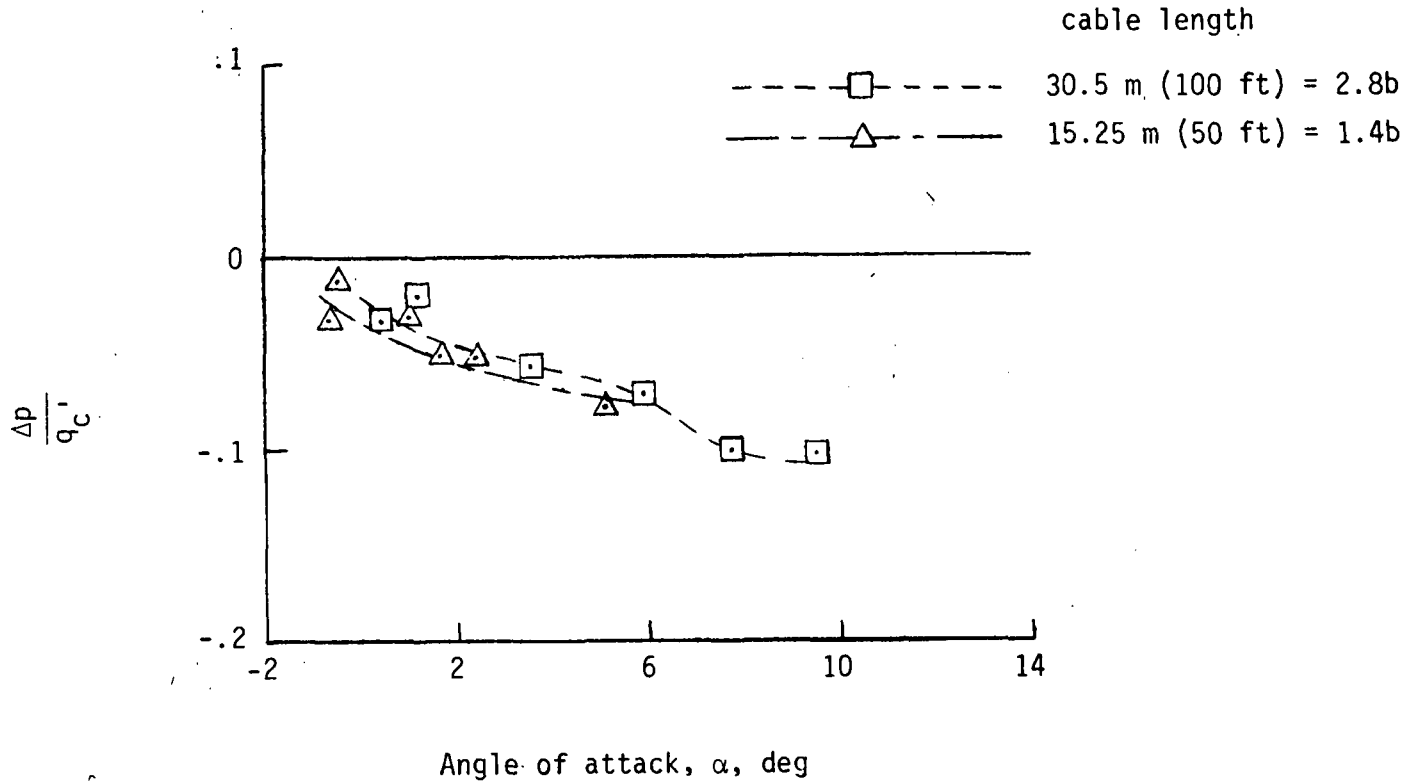

Figure 13.- Variation of static-pressure position error with angle of attack for two anemometer cable lengths. Wing-tip boom probe of airplane B. Trailing anemometer method - steady runs. Flaps down.

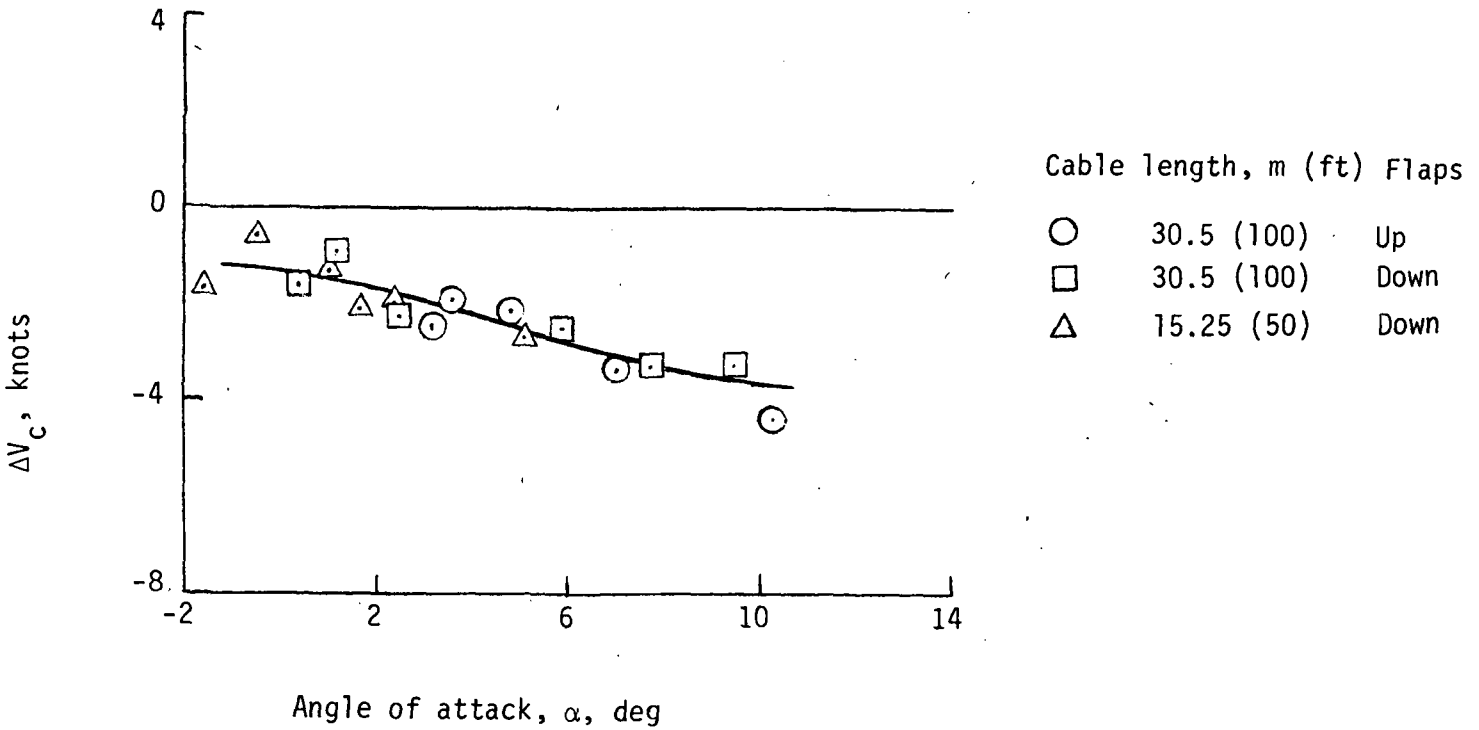

Figure 14.- Variation of airspeed error with angle of attack for two cable lengths and two flap deflections for wing-tip boom probe of airplane B. Trailing anemometer method - steady runs.

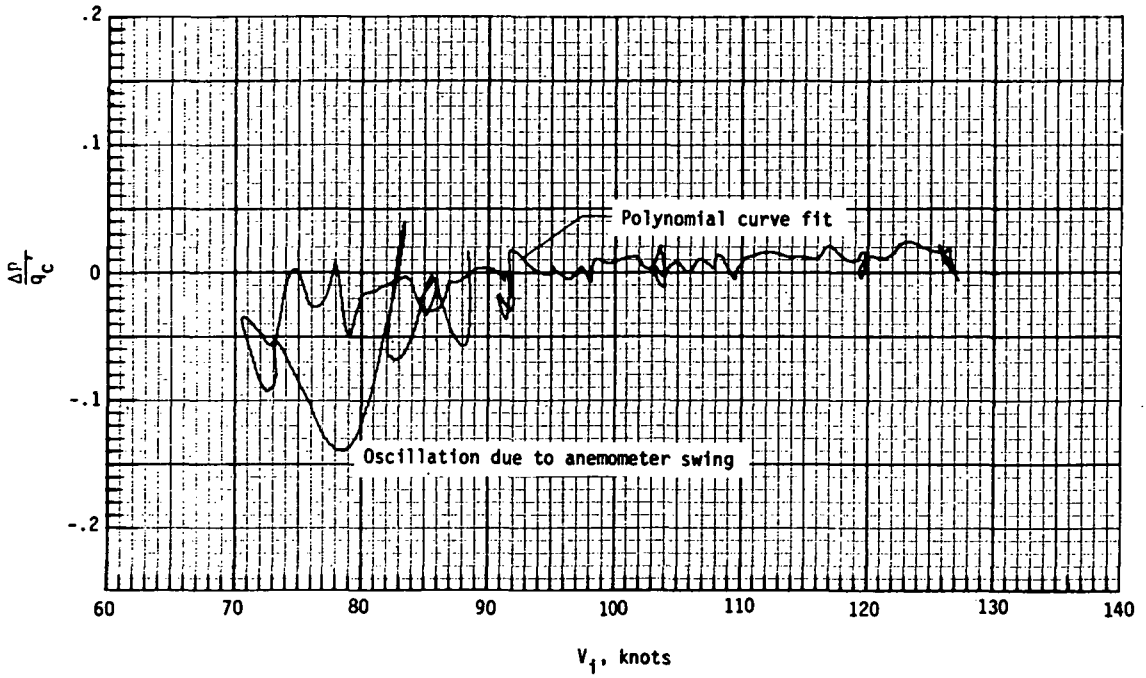

(a) Rough deceleration with anemometer swing.

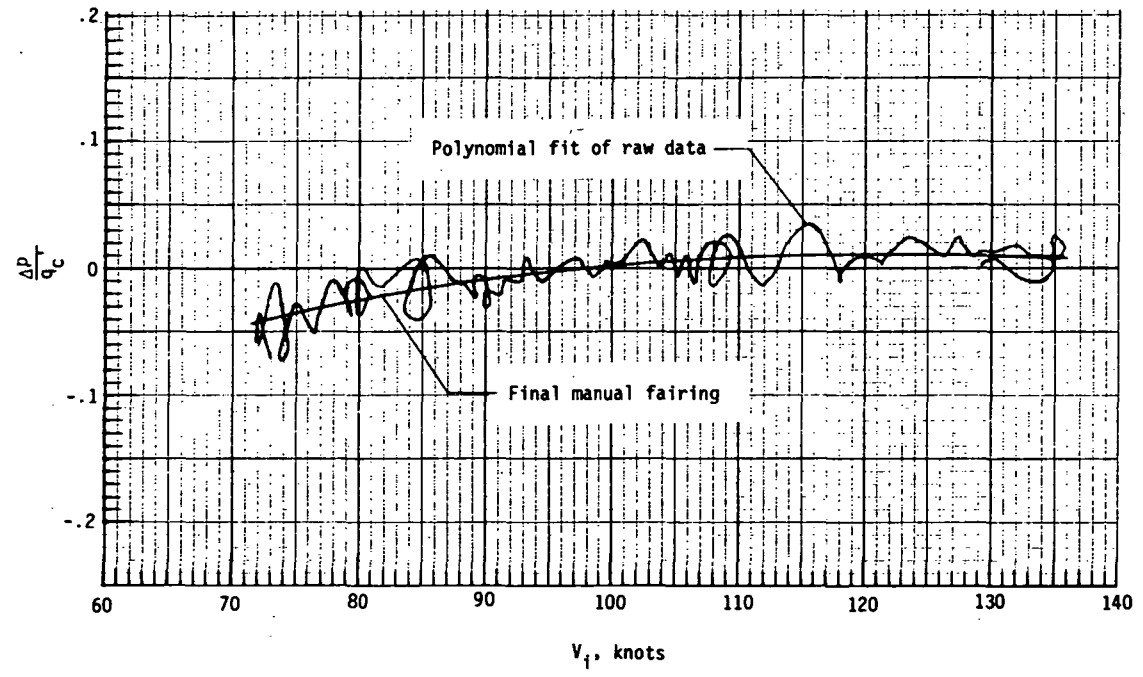

(b) Smooth deceleration.

Figure 15.- Variation of static-pressure position error with indicated airspeed for two sample deceleration maneuvers. Nose-boom probe of airplane C; cable length, 30.5 m (100 ft).

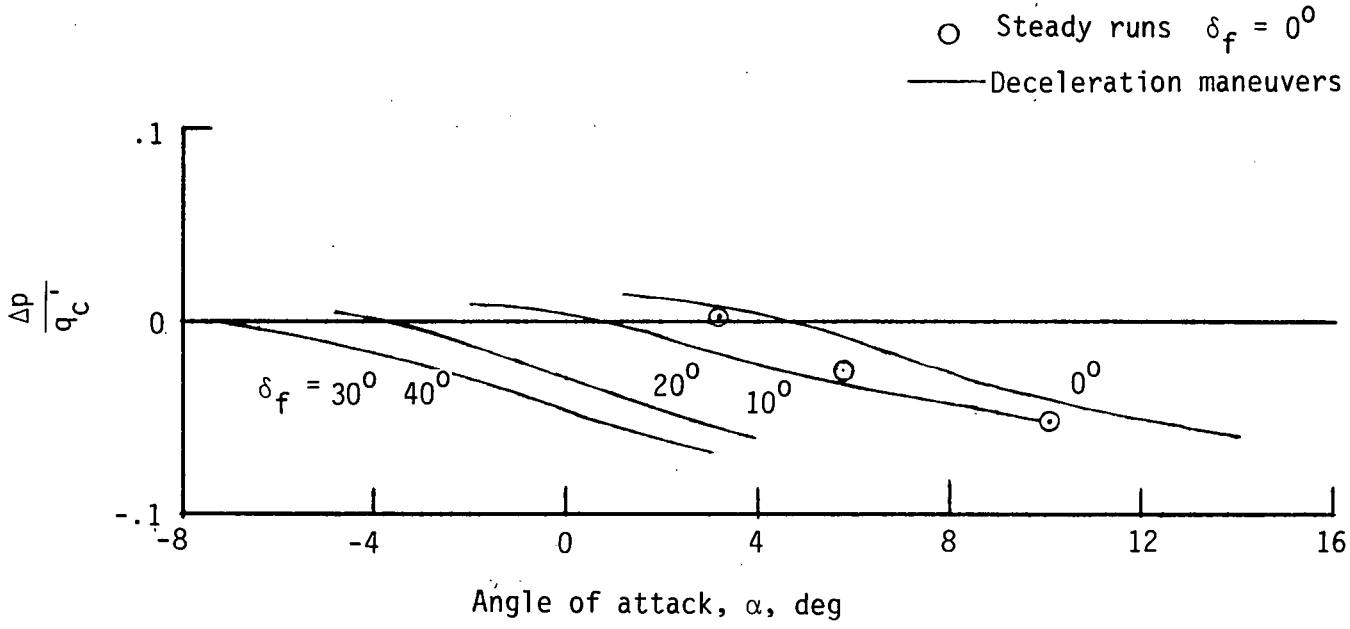

Figure 16.- Variation of static-pressure position error with angle of attack for five flap deflections for nose-boom probe of airplane C. Trailing anemometer method.

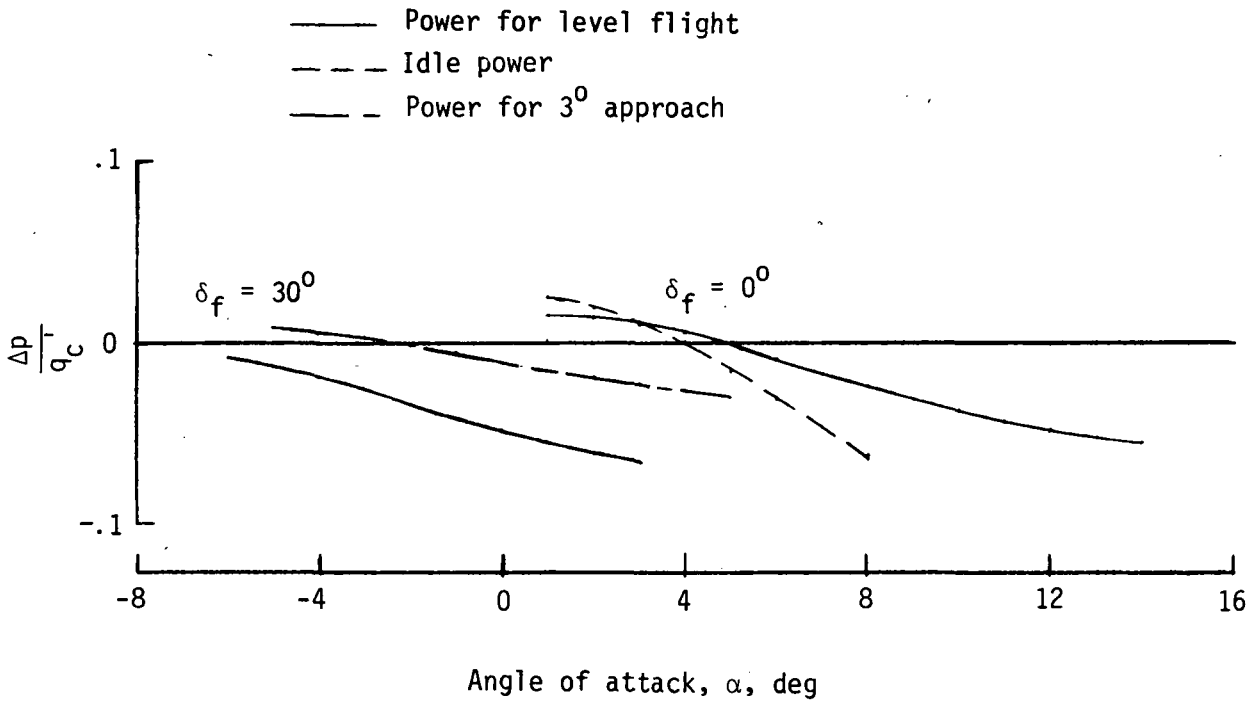

Figure 17.- Influence of engine power on static-pressure position error at two flap deflections for nose-boom probe of airplane C. Trailing anemometer method - deceleration maneuvers.

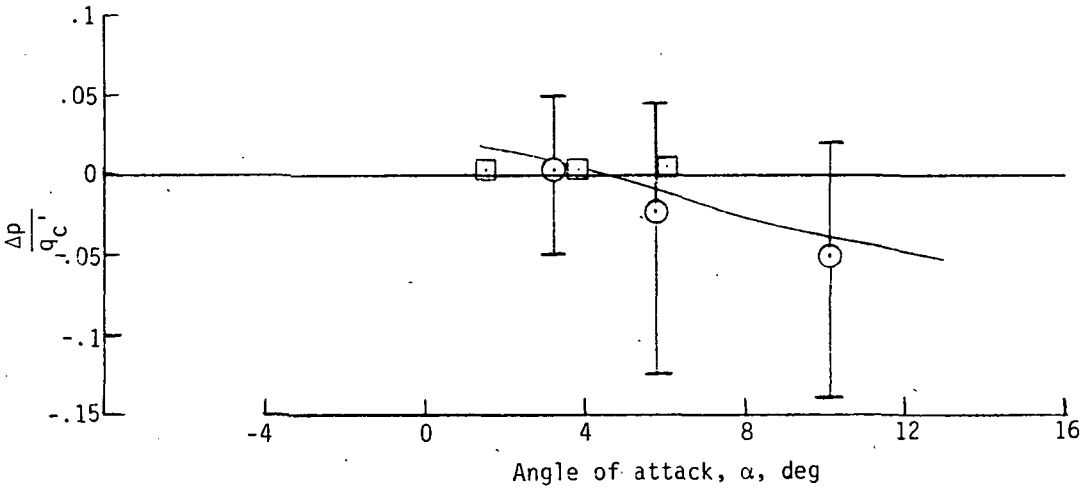

(a) Static-pressure position error.

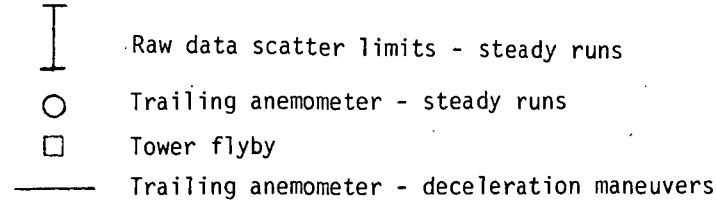

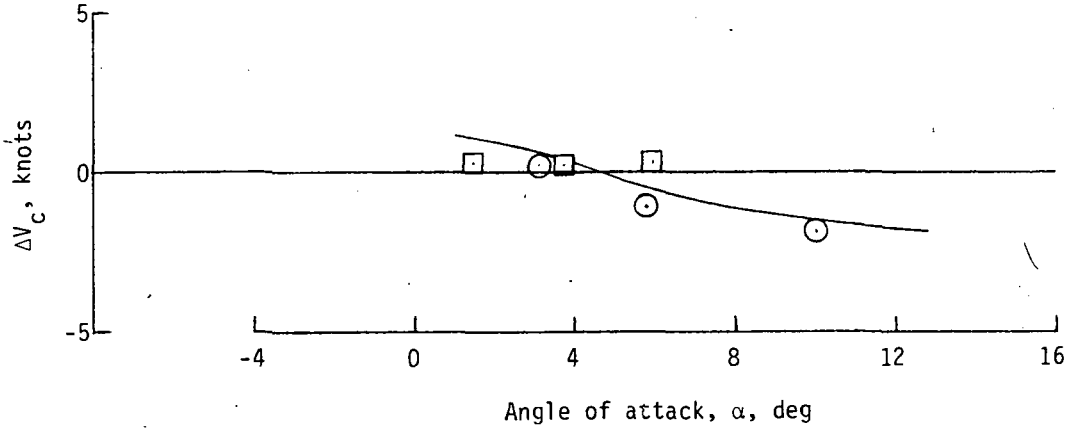

(b) Airspeed position error.

Figure 18.- Comparison of static-pressure position error measured for nose-boom probe or airplane C by trailing anemometer method (steady runs and deceleration maneuver) and tower flyby method. Flaps up.

1. Report No.	2. Government Accession No.	3. Recipient's Catalog No.
NASA TP-1135		

4. Title and Subtitle	5. Report Date
A FLIGHT EVALUATION OF A TRAILING ANEMOMETER FOR LOW-SPEED CALIBRATIONS OF AIRSPEED SYSTEMS ON RESEARCH AIRCRAFT	February 1978
	6. Performing Organization Code

7. Author(s)	8. Performing Organization Report No.
Bruce D. Fisher, Bruce J. Holmes, and H. Paul Stough III	L-11960
	10. Work Unit No.
9. Performing Organization Name and Address	505-10-13-01
NASA Langley Research Center Hampton, VA 23665	11. Contract or Grant No.
	13. Type of Report and Period Covered
12. Sponsoring Agency Name and Address	Technical Paper
National Aeronautics and Space Administration Washington, DC 20546	14. Sponsoring Agency Code

15. Supplementary Notes

16. Abstract

Research airspeed systems on three low-speed general aviation airplanes were calibrated by the trailing anemometer method. Each airplane was fitted with an NASA pitot-static pressure tube mounted on either a nose or wing boom. The uncalibrated airspeed systems contained residual static-pressure position errors which were too large for high-accuracy flight research applications. The trailing anemometer calibration was in agreement with the tower flyby calibration for the one aircraft for which the comparison was made. The continuous deceleration technique for the trailing anemometer method offers reduced test time with no appreciable loss of accuracy for airspeed systems with pitot-static system lag characteristics similar to those described in this paper.

17. Key Words (Suggested by Author(s))	18. Distribution Statement
Low airspeeds, trailing anemometer method NASA pitot-static pressure tube Static-pressure position errors Dynamic airspeed calibration Tower flyby method Airspeed calibrations	Unclassified - Unlimited Subject Category 05

19. Security Classif. (of this report)	20. Security Classif. (of this page)	21. No. of Pages	22. Price*
Unclassified	Unclassified	59	$5.25

* For sale by the National Technical Information Service, Springfield, Virginia 22161

NASA-Langley, 1978

National Aeronautics and
Space Administration

Washington, D.C.
20546

Official Business
Penalty for Private Use, $300

THIRD-CLASS BULK RATE

Postage and Fees Paid
National Aeronautics and
Space Administration
NASA-451

NASA

POSTMASTER: If Undeliverable (Section 158 Postal Manual) Do Not Return